Probing the timeline for the acquisition of altered circuit function in the developing prefrontal cortex



Marko Tvrdić

Keble College,
University of Oxford

A thesis submitted for the degree of

Master of Science by Research

Trinity Term 2022

Table of contents

Acknowledgements **5**
Statement of authorship **6**
Abstract **7**
1. INTRODUCTION **9**
1.1. Neurodevelopmental disorders 9
1.2. The medial prefrontal cortex (mPFC) 9
1.3. The mPFC and excitatory/inhibitory balance 10
1.4. GABAergic interneurons control the flow of information in the mPFC 10
1.5. Early postnatal activity of the mPFC 12
1.6. Beta and gamma oscillations are key activity patterns in the mPFC 12
1.7. Aims of this study 13
2. METHODS **14**
2.1. Generation of the *Nkx2-1-Cre:Ai32(ChR2)* transgenic line 14
2.2. Neonatal *in vivo* electrophysiology 14
2.2.1. Recordings under urethane anaesthesia 14
2.2.2. Recordings in awake animals 14
2.3. The probe and the recording protocol 15
2.4. Histology 15
2.5. High-confidence recording criteria 16
2.6. Data analysis 16
2.6.1. Detecting and characterising oscillations 16
2.6.2. Single unit isolation 16
2.6.3. Spike-LFP entrainment analysis 16
2.7. Figures and statistical analysis 17
3. RESULTS **18**
3.1. Extracellular recordings of the mouse medial prefrontal cortex during postnatal development 18
3.2. Characterising beta and gamma oscillations in anaesthesia and during development 19
3.2.1. Anaesthesia affects beta but not gamma oscillatory events pre-P12 20
3.2.2. Properties of beta and gamma oscillations in the mPFC through early postnatal development. 21
3.2.3. Postnatal day 12 is a critical juncture in the development of oscillatory activity in the mPFC 23
3.3. Single-unit activity across early postnatal development 24

3.3.1. Optogenetic tagging of Nkx2-1-derived interneurons in early postnatal mPFC 28
3.4. Spike-LFP entrainment analysis 31
3.4.1. Contribution of putative PV+ and SST+ interneurons to beta and gamma frequency oscillations 33
4. DISCUSSION **35**
References **40**

Acknowledgements

I have done this research with the help of Simon, Filippo, Gabi, members of the Lak and Packer lab, my friends in Oxford and at home and most of all, my family.

Thank you.

Statement of authorship

I declare that this thesis is my own work, however, throughout the thesis I use the pronoun "we" to indicate myself and the people below.

- Simon Butt conceptualised the project and designed the experiments.
- Armin Lak assisted with the supervision.
- Filippo Ghezzi trained me in mouse stereotaxic surgery and guided the data analysis.

Word count: 10 031

Abstract

Neurodevelopmental disorders are characterised by cognitive and behavioural deficits, which are underpinned by a broad spectrum of neural deficiencies in brain regions critical for higher-order cognition - more specifically, the medial prefrontal cortex (mPFC). The mPFC is involved in learning, memory, and decision-making, and its appropriate functioning in adulthood depends on the correct balance between excitation and inhibition established during early neural development.

GABAergic interneurons are critical components of cortical circuits where they modulate the firing of neurons and thus control information flow both in adult and developing cortical networks. The early circuits of the mPFC exhibit characteristic discontinuous oscillatory patterns in the beta and gamma frequency ranges. The precise characteristics of these early beta and gamma oscillations are unknown as well as how they relate to the activity of single neurons.

Here, we (1) explored the early oscillatory activity in the developing mPFC, (2) we examined the activity of single neurons during development, and (3) we characterised the specific interactions between beta and gamma oscillations and single neurons - with a focus on PV+ and SST+ GABAergic interneurons.

We recorded extracellularly from anaesthetised and awake animals and found that anaesthesia affects beta but not gamma oscillations and that both beta and gamma oscillations change over development - with a possible critical period at postnatal day (P) 12. Single neurons were also found to change their features during development and in anaesthesia. Through optotagging, we identified putative SST+ and PV+ interneurons and found that they differentially contribute to beta and gamma activity, as do other single neurons - with a possible critical period also at P12.

These findings shed light on the early oscillatory and single neuron activity in the mPFC and inform further investigations on the origins of neurodevelopmental dysfunctions in brain regions critical to higher-order cognition.

1. INTRODUCTION

1.1. Neurodevelopmental disorders

Neurodevelopmental disorders such as autism spectrum disorder, attention deficit hyperactivity disorder and intellectual disability are characterised by defects in social interaction, cognition, emotional and motor processing (American Psychiatric Association, 2013, Parenti et al., 2020). Estimates suggest that more than 3% of children are affected by neurodevelopmental disorders (Gilissen, et al. 2014). Due to a broad spectrum of genotypic and phenotypic heterogeneities in these disorders effective treatments are still lacking (Parenti et al., 2020). A region of the brain critically affected in many neurodevelopmental disorders is the medial prefrontal cortex (Schubert et al., 2015).

1.2. The medial prefrontal cortex (mPFC)

The medial prefrontal cortex (mPFC) is considered to be the core processing unit of the cerebral cortex for higher-order cognition. It is involved in a number of cognitive abilities such as learning (Pasupathy and Miller., 2005), memory (Warden and Miller, 2010), cognitive flexibility (Clarke et al., 2004, Gruber et al., 2010), attention (Bissonette and Powell, 2012, Kim et al., 2016) and decision making (Abbas et al., 2018; Le Merre et al., 2021). Many of these abilities are impaired in neurodevelopmental disorders (Schubert et al., 2015).

The mPFC receives multimodal input from sensory areas, limbic and neuromodulatory brain nuclei (Carmichael and Price, 1996; Hoover and Vertes, 2007) and processes these diverse inputs – along a distinct set of anatomically-defined prefrontal areas – to direct behaviour (Ferguson and Gao, 2018). The mPFC can be subdivided, based on cellular composition, along the dorsoventral axis into the anterior cingulate cortex, the prelimbic cortex, and the infralimbic cortex. Although the functional significance of these cytoarchitectural subdivisions remains unclear, anatomical subdivisions can be delimited by afferent and efferent connectivity motifs with other cortical and subcortical brain regions (Le Merre et al., 2021). Anatomically tracking these connections revealed a complicated network of mPFC projections (Ahrlund-Richter et al., 2019). While some are unidirectional, most of these projections are reciprocal, effectively allowing the mPFC to direct a wide range of behaviours by continuously synchronising incoming neural activity (Le Merre et al., 2021).

There are some critical differences between the mPFC and other cortical areas (Anastasiades and Carter, 2021). The mPFC is agranular – it does not contain a canonical layer (L) 4 that receives thalamic input - instead, thalamic input is received across L1, L2/3, L5, and L6. Also, there is a different distribution of inhibitory interneurons - likely creating computational abilities distinct from other cortical areas (Anastasiades and Carter, 2021).

1.3. The mPFC and excitatory/inhibitory balance

The adult function of mPFC depends on accurate cellular computations evoked in response to sensory and internally-generated signals. How this arises during development and how it is maintained through adulthood is poorly understood. However, it is reliant on interactions between excitatory pyramidal projection neurons and locally-projecting GABAergic inhibitory interneurons, forming balanced networks that underpin information processing in the PFC and onward relay to other brain areas for the enactment of voluntary behaviour.

The mechanisms of maintenance of excitatory/inhibitory (E/I) balance in adulthood are multidimensional and complex; however, they are dynamically adjusted to prevent runaway excitation or discontinuation of activity in response to varying input strength (Wehr and Zador, 2003, Pouille et al., 2009). These mechanisms act across spatial and temporal scales. For example, E/I balance is maintained at the level of single neurons and neural circuits. At the level of single neurons, excitatory and inhibitory synapses are specified and maintained by various mechanisms (Iascone et al., 2020). At the level of neural circuits, different homeostatic mechanisms act to buffer neuronal activity during prolonged stimuli (Hengen et al., 2013).

Accurate information processing, underpinned by a functional E/I balance, is critical for appropriate cognitive functioning. Manipulations of E/I balance in the mPFC have been shown to disrupt social behaviour and sensory perception (Shen et al., 2011). Additionally, subtle imbalances between excitation and inhibition in neural circuits of the mPFC have been proposed as an aetiological model of psychiatric dysfunction in neurodevelopmental disorders (Rubenstein and Merzenich, 2003).

This indicates a critical link between the mPFC function and higher-order cognitive deficits and points to a need to better understand the longitudinal development of the mPFC at the level of neural circuits and individual neurons.

1.4. GABAergic interneurons control the flow of information in the mPFC

A critical component of neural circuits in the mPFC, as in other cortical areas, are GABAergic interneurons. The activity of GABAergic interneurons plays an essential role in information processing in the cortex – by coordinating the synchronous firing of excitatory pyramidal neurons to enable information transfer (Cobb et al., 1995). Additionally, they provide the neural circuits with computational flexibility, which enables a diverse repertoire of possible neuronal responses (Isaacson and Scanziani, 2011).

GABAergic interneurons are found across prefrontal cortical layers and have distinct morphological and physiological characteristics that strongly influence their effect on local circuitry (Nahar et al., 2021). In this project, we focus on two subtypes of GABAergic interneurons thought to be essential for the control of early cortical activity.

Firstly, parvalbumin-expressing (PV+) interneurons form perisomatic contacts (Anastasiades and Carter, 2021) to regulate pyramidal cell output. Adult PV+ interneurons are described as fast-spiking due to their fast, *Kv3.1*-mediated rectification and narrow spike waveform. This enables them to fire in short bursts at a high frequency (Nahar et al., 2021).

Secondly, somatostatin-expressing (SST+) interneurons – a subtype with important roles in early development ranging from synapse formation to driving neuronal maturation and which, in adults, have slower spike kinetics when compared to PV+ interneurons, a more depolarised membrane potential and higher input resistance (Riedemann, 2019). Furthermore, SST+ interneurons primarily inhibit the dendrites of pyramidal cells and PV+ interneurons (Anastasiades and Carter, 2021).

During embryonic development, GABAergic interneurons originate from the ganglionic eminences of the ventral telencephalon and migrate tangentially into the cortex (Lim et al., 2018) to reach and integrate with locally-born excitatory pyramidal neurons (Greig et al., 2013). The appropriate developmental trajectory of GABAergic interneurons, where the numbers, locations, and morphologies are correctly assigned and specified, sets up these circuits to support physiological early neural activity.

Both PV+ and SST+ interneurons play critical roles in establishing early circuits. During the first three postnatal weeks, the strength of somatostatin-pyramidal connections decreases while the strength of PV-pyramidal connections increases (Chini and Hanganu-Opatz, 2020) - effectively modulating the activity in the early postnatal mPFC.

Additionally, PV+ and SST+ interneurons derived from the *Nkx2-1*-expressing domain of the ventral telencephalon form functional connections even before the emergence of excitatory pyramidal networks, and during development, they engage in transient circuits across the neocortex (Anastasiades and Marques-Smith et al., 2016). This suggests that both PV+ and SST+ interneurons play a crucial role in regulating cortical activity during the early postnatal period.

1.5. Early postnatal activity of the mPFC

Recent efforts have pointed towards oscillations in the local field potential (LFP) to be critical activity patterns in the establishment, maintenance, and functions of early prefrontal cortical networks.

Oscillations are recurrent patterns of local field potential activity originating from the spatiotemporal summation of transmembrane currents (Buzsaki et al., 2012), i.e., synchronous activation of local neuronal populations.

An oscillatory event, defined by an averaged depolarised and hyperpolarised cycle, effectively allows a window for neurons to synchronise their firing (Buzsaki and Draguhn, 2004) and possibly provide an "activity scaffold" for communication within and between brain areas (Buzsaki and Llinas, 2017, Le Merre et al., 2021).

Important functional hallmarks characterise the early prefrontal activity in mice. The first two postnatal weeks are dominated by intermittent periods of electrical silence (defined by an isoelectric LFP trace) and brief periods of bursting activity (Chini and Hanganu-Opatz, 2021). This discontinuous activity does not appear in adult brains and consistently appears across cortical areas. Additionally, this phenomenon is evolutionarily conserved across species - observed in EEG traces of newborn humans (Vanhatalo and Kaila, 2006) and rodents (Chini and Hanganu-Opatz, 2021).

1.6. Beta and gamma oscillations are key activity patterns in the mPFC

A wealth of recent studies point toward the mPFC being a brain region with a particularly strong oscillatory activity - and oscillations in the gamma and beta frequency ranges have been associated with a number of behavioural states and cognitive abilities in adult animals (Sohal, 2016).

Gamma oscillations (40-80 Hz) are primarily induced by interneurons (Cardin et al., 2009), and they have been causally linked to higher-order processing in attention (Kim et al., 2016) and cognitive flexibility in adults (Cho et al., 2015).

The synchronised firing of fast-spiking parvalbumin-expressing interneurons driven by periodic light stimulation has been shown to generate gamma oscillations in the cortex (Cardin et al., 2009) and inhibition of parvalbumin-expressing interneurons suppressed gamma oscillations *in vivo* (Sohal et al., 2009).

Interestingly, while inhibition may be sufficient to generate activity in the gamma range, rapid gamma activity modulation requires both excitation and inhibition to be proportionately balanced during each gamma oscillation cycle – suggesting a dynamic interplay between excitatory and inhibitory neurons in the "fine-grained" modulation of gamma activity (Atallah and Scanziani, 2009).

During cortical development, gamma activity is transient (Khazipov et al., 2013) and increases in prominence during the second postnatal week (Bitzenhofer et al., 2020). However, it remains unclear how the characteristics of gamma events change during development.

By contrast, oscillations in the beta frequency range have been observed across cortical areas and in the mPFC have been associated with executive control of action and working memory in adults (Stanley et al., 2018).

During development, discontinuous bursts of beta frequency activity (spindle bursts) originating from the thalamus have been described and characterised in sensory cortices. They have been proposed to organise spiking activity (Colonesse and Khazipov, 2012) and direct the development of sensory processing (Ackman et al., 2012, Chini and Hanganu-Opatz, 2021). In the mPFC, the developmental features of this type of activity are less clear.

While the link between GABAergic interneurons and oscillatory activity in the adult mPFC has been established, it is not entirely clear how this arises through development. PV+ interneurons have been shown to mature in line with increasing gamma frequency activity in the developing mPFC (Bitzenhofer et al., 2020); however, in the absence of PV+ interneurons during the early postnatal period, the origins of high-frequency activity in the gamma range are unknown. SST+ interneurons have been shown to regulate the development of thalamocortical connections (Tuncdemir et al., 2016), and in the visual cortex, suppression of SST+ interneurons disrupted beta activity (Chen G, Zhang Y, Li X, et al., 2017). However, it remains unknown how PV+ and SST+ interneurons specifically contribute and interact with beta and gamma oscillations during the development of the mPFC.

1.7. Aims of this study

In this study, we aim to address important gaps in the knowledge regarding early prefrontal beta and gamma oscillations and single neurons, more specifically PV+ and SST+ interneurons.

Specifically, we aimed to (1) examine the specific features of beta and gamma activity, such as their duration and frequency of occurrence, in the developing mPFC. (2) We aimed to optogenetically identify PV+ and SST+ interneurons derived from the *Nkx2-1*-expressing domain of the telencephalon and, more generally, characterise the development of single unit activity in the mPFC. (3) We aimed to analyse the entrainment and recruitment of single units in beta and gamma frequency oscillations over time, focusing on PV+ and SST+ interneurons.

Together, this analysis will provide a detailed description of the early oscillatory and single unit activity and a perspective on the interactions between GABAergic interneurons and early network oscillations in the developing mPFC.

2. METHODS

2.1. Generation of the *Nkx2-1-Cre:Ai32(ChR2)* transgenic line

To enable optogenetic activation and identification of somatostatin-expressing (SST+) and parvalbumin-expressing (PV+) GABAergic interneurons, we utilised the *Nkx2-1-Cre* transgenic line. The *Nkx2-1-Cre* transgenic line selectively labels cortical SST+ and PV+ GABAergic interneurons derived from the medial ganglionic eminence (Xu et al., 2008).

Males with the *Nkx2-1-Cre* transgenic were crossed with females homozygous for the *Ai32(ChR2)* reporter allele to generate *Nkx2-1Cre:Ai32(ChR2)* pups that have *Channelrhodopsin2* in SST+ and PV+ cortical GABAergic interneurons.

2.2. Neonatal *in vivo* electrophysiology

Mouse pups of both sexes (P8-P21) were recorded. In addition, pup weights, fur type, and eyes closed/open were noted. All mice were recorded only once.

2.2.1. Recordings under urethane anaesthesia

Pups were anaesthetised using urethane anaesthesia (1-2 mg/kg) injected intraperitoneally in 3-4 doses (1 dose = ¼ of maximum urethane dose for pups of 2 mg/kg) in 20-minute intervals until the tail, and pedal reflex responses disappeared. Atropine (0.1 mg/kg) was injected subcutaneously immediately following the first urethane injection. Atropine was added to the anaesthetic protocol to reduce bronchial secretions and prevent drops in heart rate caused by anaesthesia. Pedal and tail reflexes were monitored throughout the anaesthesia induction to estimate the depth of anaesthesia.

After the pedal and tail reflexes disappeared, the animal was scalped and fixed in the stereotaxic device with the incorporated heating pad to provide thermoregulation during the procedure. Next, the skull periosteum was dissolved using a 3% hydrogen peroxide solution, and the skull was cleaned with saline.

Two craniotomies were performed; one above the mPFC (~1.3-1.5 mm anterior and 0.3-0.5 mm lateral to bregma for P8-P12 and ~1.7-1.9 mm anterior and 0.3-0.5 mm lateral to bregma for P15-P21) for the probe and one above the contralateral cerebellum for the ground wire (ground wire was inserted between the brain and the skull).

2.2.2. Recordings in awake animals

Only pups younger than/or P12 were used to perform awake recordings due to the acute nature of the recordings. In addition, mouse pups are not habituated to head fixation, and as they grow in mass, the risk of the head-fixation apparatus currently available in the lab detaching from the skull increases.

Pups were anaesthetised using isofluorane (in 100% oxygen, 4.5% for induction, 2-3% for maintenance - higher for younger animals). Tail and pedal reflexes were monitored throughout the anaesthetic protocol. Pups were scalped, and the periosteum was cleaned as described above.

Plastic bars were placed on the nasal and occipital bones and secured with dental cement. To minimise muscle/movement artefacts in the recording, pups' neck muscles were cut.

Two craniotomies were performed; one above the mPFC (~1.3-1.5 mm anterior and 0.3-0.5 mm lateral to bregma) for the probe and one above the posterior contralateral cortex for the ground wire (ground wire was inserted between the brain and the skull). The ground wire was not placed in the contralateral cerebellum but the contralateral cortex due to the high amount of dental cement used to cover the posterior skull.

2.3. The probe and the recording protocol

All recordings were performed using a single-shank 32-channel silicon probe with the incorporated optic fibre (A1x32-Poly2–5mm-50s-177, Neuronexus, US) to enable effective blue light delivery and stimulation of local neurons. Before insertion, the probe was dipped in 1,1′-dioctadecyl-3,3,3′,3′-tetramethylindocarbocyanine perchlorate (DiI, Vybrant™ DiI Cell-Labeling Solution, ThermoFisher) and left to dry for 20 seconds three times to enable *post hoc* identification of probe location. Then, the probe was inserted slowly (~3 µm/s) using an analog micromanipulator (SOLO-50, Sutter Instruments, US) at an approximate depth of 1900µm from the cortical surface. Data was sampled at 30000 Hz using an OpenEphys acquisition board.

Before recording, mice were left to recover for a minimum of 20 minutes to ensure reliable capture of the local field potential (LFP) and maximise unit acquisition. The recording protocol entailed 60 minutes of baseline activity acquisition followed by blue light stimulation.

Optogenetic spike-tagging was performed through a fibre-coupled blue (472 nm) laser connected to an optoelectrode. Long-duration (50 ms) laser pulses accounted for reduced excitability of *ChR2* during early postnatal development. One optogenetic session, characterized by 100 laser pulses delivered at 0.1 Hz frequency, was conducted immediately after the baseline activity acquisition.

Following signal acquisition, pups were decapitated, and their brain was extracted and incubated in 4% paraformaldehyde (PFA) solution for 48-96h at 4°C.

2.4. Histology

To enable histological identification of probe location, the probe was dipped in DiI as described above. Following incubation in PFA, brains were fixed in 2% agarose gel and sliced on the vibratome (Leica VT1000s) at 100 µm thickness. Slices were then incubated in a 4′,6-diamidino-2-phenylindole (DAPI, Sigma-Aldrich) solution (5 µg/mL in PBS) for ~5 minutes and then washed with PBS (pH: 7.2-7.6, 0.01M).

Slices were then mounted and fixed using a liquid mounting medium (Fluoromount-G™, ThermoFisher), covered with a cover slide, and fixed in place with nail polish. Mounted slices were then imaged using a fluorescent microscope (Leica epifluorescence microscope with a CY5 filter cube), and images were acquired using a Leica DFC500 camera with FireCam software. Finally, individual images were processed and merged in Fiji (Schindelin et al., 2012).

2.5. High-confidence recording criteria

To determine which animals can be included in the final dataset, a set of criteria was developed: (1) the animal needs to be of appropriate weight, and it needs to have its eyes closed or open depending on its age (P13 - eye-opening (Greenham and Greenham, 1977), (2) the surgery needs to be deemed as high quality (minimal bleeding, short surgery time), (3) mPFC probe location needs to be confirmed histologically and (4) the recording needs to contain at least one single unit.

2.6. Data analysis

2.6.1. Detecting and characterising oscillations

To automatically detect oscillatory events, we utilised a computational approach called envelope thresholding. Envelope thresholding is a signal processing method and was adapted here in several key steps: (1) the raw LFP signal was bandpass filtered in the desired frequency range (10-35 Hz for beta events and 40-80 Hz for gamma events), (2) the envelope of the signal was defined as the real part of the Hilbert transform. Beta and gamma events were defined as segments of the envelope larger than 2x the standard deviation of the envelope with a duration longer than 0.1s.

Characteristics of beta and gamma events, such as frequency of occurrence and duration, were extracted using custom-built MATLAB code. Local field potentials and spectrograms were acquired using NeuroScope2 (Petersen et al., 2021)

2.6.2. Single unit isolation

Automatic spike sorting was conducted using Kilosort2 (Pachitariu et al., 2016). The sorted clusters were then visualised and manually curated using Phy2 (Rossant et al., 2016) to identify single units, multi-unit activity, and noise. To classify a cluster as a single unit, the cluster needs to: (1) stably fire for at least 10 minutes, (2) have a clear and consistent waveform, (3) have less than 1‰ of spikes violating the refractory period (approximated by Phy2), (4) be dissimilar from other clusters in their spike waveform characteristics.

2.6.3. Spike-LFP entrainment analysis

Following LFP bandpass filtering and calculation of the Hilbert transform of the signal, phases of the oscillation were extracted using the *angle* function in MATLAB. Pairwise-phase consistency was computed as the cosine of the absolute angular distance for all given pairs of relative phases of the spike timing in relation to the LFP, as described in Vinck et al., 2010. The PPC method of spike-LFP coupling is more robust than in data containing a smaller number of spikes (Veit et al., 2017) and, as such, is suitable to use in the analysis of neonatal electrophysiological datasets.

Significance was evaluated using the Raleigh test of circular uniformity. Circular histograms were created using the *circ_plot* function in MATLAB.

The inter-spike interval (ISI) shuffle method was used as described in Narayanan and Laubach, 2009. This method defines oscillatory events (here using envelope thresholding, see above) and then shuffles the inter-spike intervals 1000 times (to obtain the null distribution). The probability of spikes within oscillatory events is a measure to obtain a distribution of shuffled spike probability. A unit was classified as entrained by an oscillatory event if the real spike probability was greater than the null distribution in at least 99.9% of cases.

2.7. Figures and statistical analysis

Data processing was done in MATLAB (R2021b, MathWorks). Schematics were created using Biorender, and plots were created using GraphPadPrism (GraphPad Prism version 8.0.0). Statistics were run using MATLAB and GraphPadPrism. Normality of data was examined using the Shapiro-Wilk test ($p<0.05$).

3. RESULTS

3.1. Extracellular recordings of the mouse medial prefrontal cortex during postnatal development

Extracellular silicon probe recordings were done in the medial prefrontal cortex (mPFC) of 45 mouse pups ranging from postnatal day (P) 7 to P24 (Figure 1). Postnatal mPFC stereotaxic coordinates previously described in the literature (Bitzenhofer et al., 2020) failed to successfully target this cortical region in the *Nkx2-1Cre;Ai32* background (*C57Bl/6*) used in our experiments. However, through trial and error and reconstruction of DiI tracts (Figure 1C), we established a set of coordinates that allowed reliable targeting of mPFC across the ages tested in the current study (Figure 1A). Extracellular recordings were performed at a depth of 1.9 mm from the surface of the cortex using a 32-channel electrode with the attached optic fibre to enable optical stimulation of *Channelrhodopsin2* conditionally expressed in *Nkx2-1*-derived GABAergic interneurons and thereby allow optogenetic tagging (Valero et al., 2021) and identification of interneuron spike waveforms (Figure 1BC). A priori *high-confidence recording criteria* (see Methods) were applied to all recordings, resulting in 20 mouse pups reaching the threshold for inclusion in the final dataset; these included local field potential (LFP) recordings from three awake neonatal (P8-P12) animals, nine urethane-anaesthetised neonatal (P8-P12) animals and eight urethane-anaesthetised juvenile (P15-P21) animals (Figure 1D), and six hundred identified single-units.

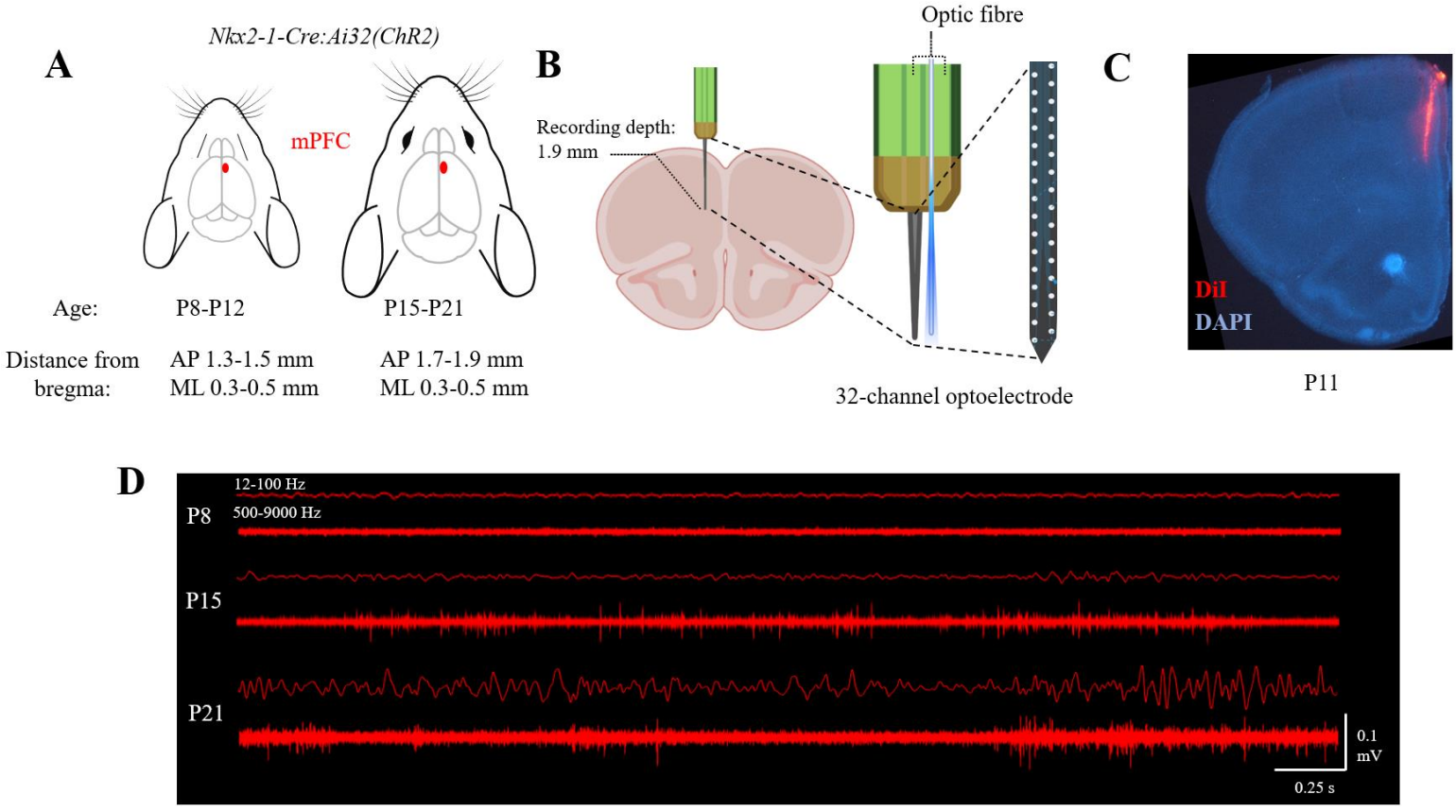


Figure 1: Early postnatal extracellular recordings of the mPFC and the development of neural activity in the mPFC. A. Experimentally determined stereotaxic coordinates for targeting the mPFC of neonatal (P8-P12) and juvenile (P15-P21) *Nkx2-1-Cre:Ai32(ChR2)* mice. **B.** Diagram shows a coronal section through the mouse brain at the level of the mPFC showing the orientation of the 32-channel silicon probe and the attached optical fibre. **C.** *Post-hoc* histology enabled us to confirm the location of the DiI-coated probe in the mPFC. **D.** Representative examples of extracellular recordings of the local field potential (LFP, 12-100 Hz) and multi-unit activity (MUA, 500-9000 Hz) after bandpass filtering, obtained at postnatal day (P)8 (top traces), P15 (middle traces) and P21 (bottom traces).

3.2. Characterising beta and gamma oscillations in anaesthesia and during development

Envelope thresholding algorithm (Figure 2A) was used to detect oscillatory activity in LFP in the beta (10-35 Hz) (Figure 2B), and gamma (40-80 Hz) (Figure 2C) frequency ranges both in head-fixed and anaesthetised animals through development (P8-P21).

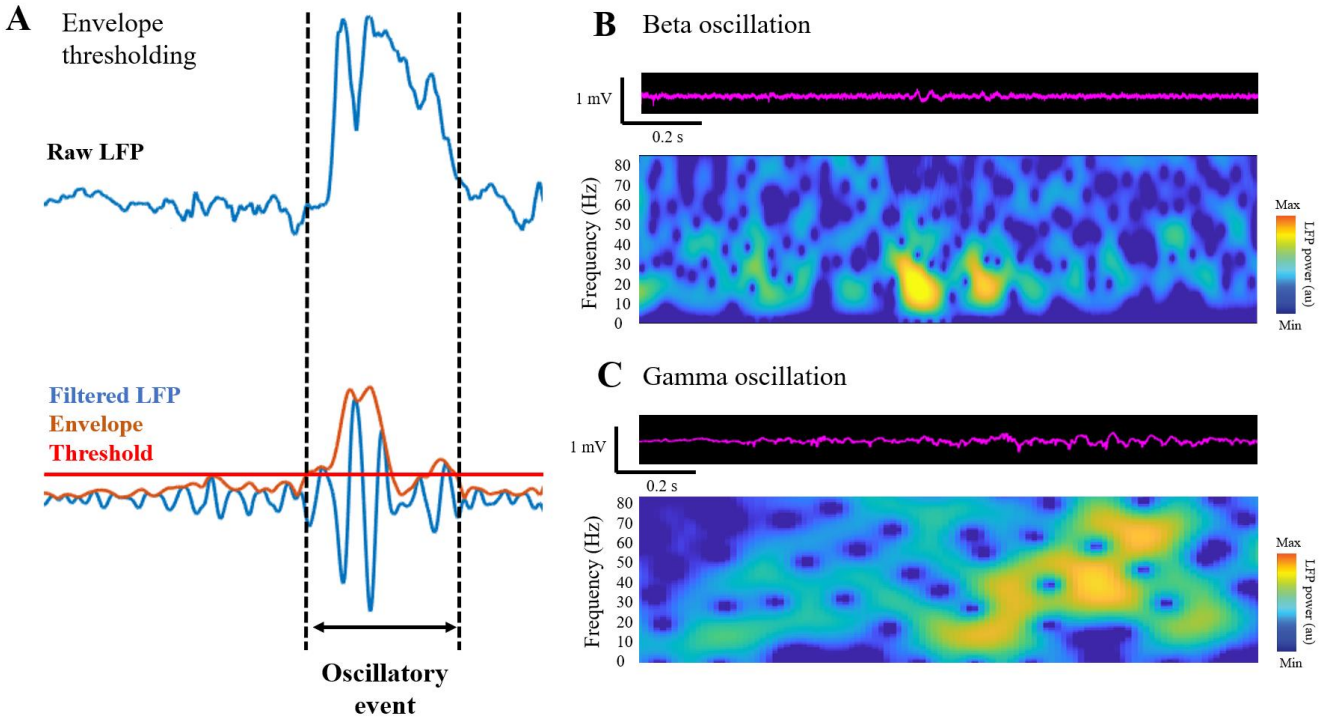


Figure 2: Envelope thresholding algorithm and representative beta and gamma activity at P11. A. Envelope thresholding algorithm: the top trace shows the raw LFP with the bandpass filtered (here shown 10-35 Hz event) LFP and the corresponding envelope (orange line) and threshold (red straight line; 2x standard deviation of the envelope). **B.** An example LFP trace showing an oscillation in the beta frequency range lasting ~0.2 seconds with the corresponding spectrogram shown below. **C.** Similar data to (B) but for a gamma frequency oscillation lasting ~0.3 seconds. LFP traces and spectrograms were obtained in Neuroscope2 (Petersen et al., 2021). Raw LFP trace was bandpass filtered (10-4000 Hz), and the spectrograms were constructed with a 0.1 s window width and a 1 Hz step size.

3.2.1. Anaesthesia affects beta but not gamma oscillatory events pre-P12

To examine the effects of urethane anaesthesia on early mPFC activity, we recorded from both awake, head-fixed (N=3) and urethane-anaesthetised (N=9) neonatal (P8-P12) animals.

Urethane was used as an anaesthetic for two reasons: (1) effects of urethane on the brain are thought to resemble sleep states (Clement et al., 2008), the dominant behavioural state of neonates (Rensing et al., 2018). However, using urethane as a proxy for natural sleep has recently been disputed as it has been shown that urethane anaesthesia induced burst suppression activity patterns – types of activity absent in unanaesthetised pups (Gomez et al., 2022). Beyond the behavioural state, (2) optical intrinsic signal imaging *in vivo* experiments have shown that urethane alters the sensory evoked response and local blood flow less than isoflourane in the somatosensory cortex – another method of non-recovery anaesthesia (Shumkova et al., 2021).

Analysis of the LFP focused on the frequency of occurrence, mean durations, and overall percentage time spent in beta - corresponding to discontinuous spindle burst and gamma-frequency oscillations. Due to the low sample number of awake neonatal animals (N=3), the comparisons made in this case are likely underpowered.

Urethane anaesthesia significantly increased the frequency of occurrence of beta oscillations (unpaired t-test: $t(10) = 2.826$, $p = 0.018$) compared to awake head-fixed pup, but had no effect on the mean duration (unpaired t-test: $t(10) = 1.647$, $p = 0.1305$) nor on the overall time spent in the beta frequency oscillation range (unpaired t-test: $t(10) = 1.484$, $p = 0.1686$) (Figure 3A). Our anaesthesia regime had no effect on the frequency of gamma occurrence (unpaired t-test: $t(10) = 2.179$, $p = 0.0543$), the mean duration of gamma events (unpaired t-test: $t(10) = 0.085$, $p = 0.93$) nor overall time spent in gamma frequency oscillations compared to control, head-fixed animals (unpaired t-test: $t(10) = 1.804$, $p = 0.1014$) (Figure 3B).

This suggests that urethane affects some aspects of discontinuous, low-frequency but not high-frequency oscillations early in mPFC development.

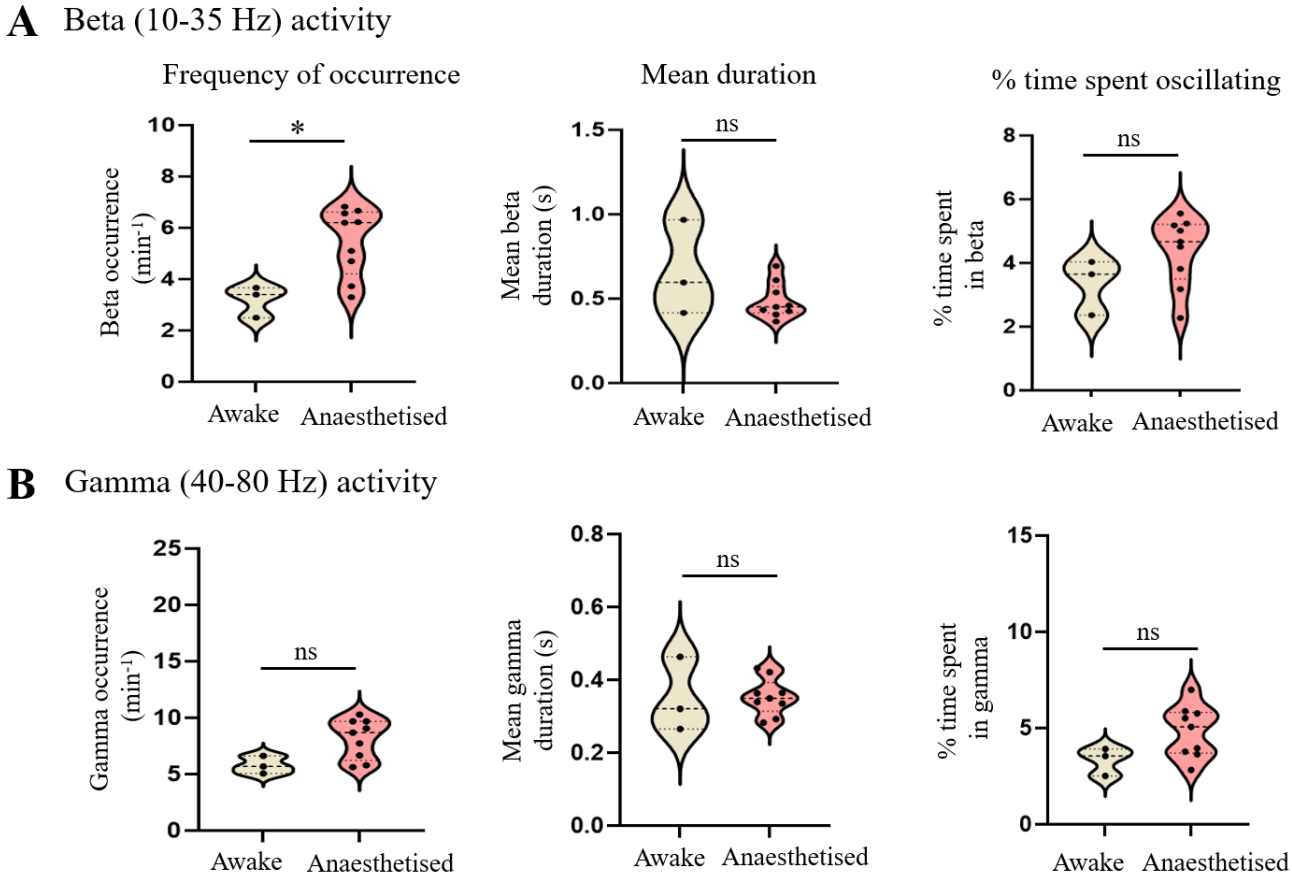


Figure 3: The effect of anaesthesia on oscillatory activity in P8-P12. Violin plots showing the frequency of occurrence, mean duration, and % time spent oscillating in (**A**) beta and (**B**) gamma frequency oscillations in awake and urethane-anaesthetized animals. Dashed lines in the violin plots indicate the median, while the dotted lines indicate the quartile values. Asterisks above the plots indicate a significant difference between states (*=p<0.05), while ns indicates no-significant difference at $\alpha = 0.05$ (p>0.05).

3.2.2. Properties of beta and gamma oscillations in the mPFC through early postnatal development.

Having characterised the effect of urethane anaesthesia early in development, we now moved to examine how oscillatory activity in the mPFC varies through development. We compared the frequency of occurrence, mean durations, and overall percentage of time spent in beta and gamma between neonatal (P8-P12, N=9) and juvenile (P15-P21, N=8) urethane-anaesthetised animals.

There was no relationship between age and the frequency of occurrence of beta oscillations (unpaired t-test: $t(15) = 1.602$, $p = 0.1301$), but there was a decrease in the duration of individual beta events (unpaired t-test: $t(15) = 3.763$, $p = 0.0019$) and the percentage of time each animal spent in the beta frequency range (unpaired t-test: $t(15) = 4.099$, $p = 0.0009$) (Figure 4A). In contrast, the occurrence of gamma frequency oscillations increased (unpaired t-test: $t(15) = 3.044$, $p = 0.0082$) while the mean duration (unpaired t-test: $t(15) = 1.93$, $p = 0.0727$) and the percentage of time spent in gamma oscillations (unpaired t-test: $t(15) =$

1.809, p = 0.0905) did not differ significantly over the developmental period studied (Figure 4B).

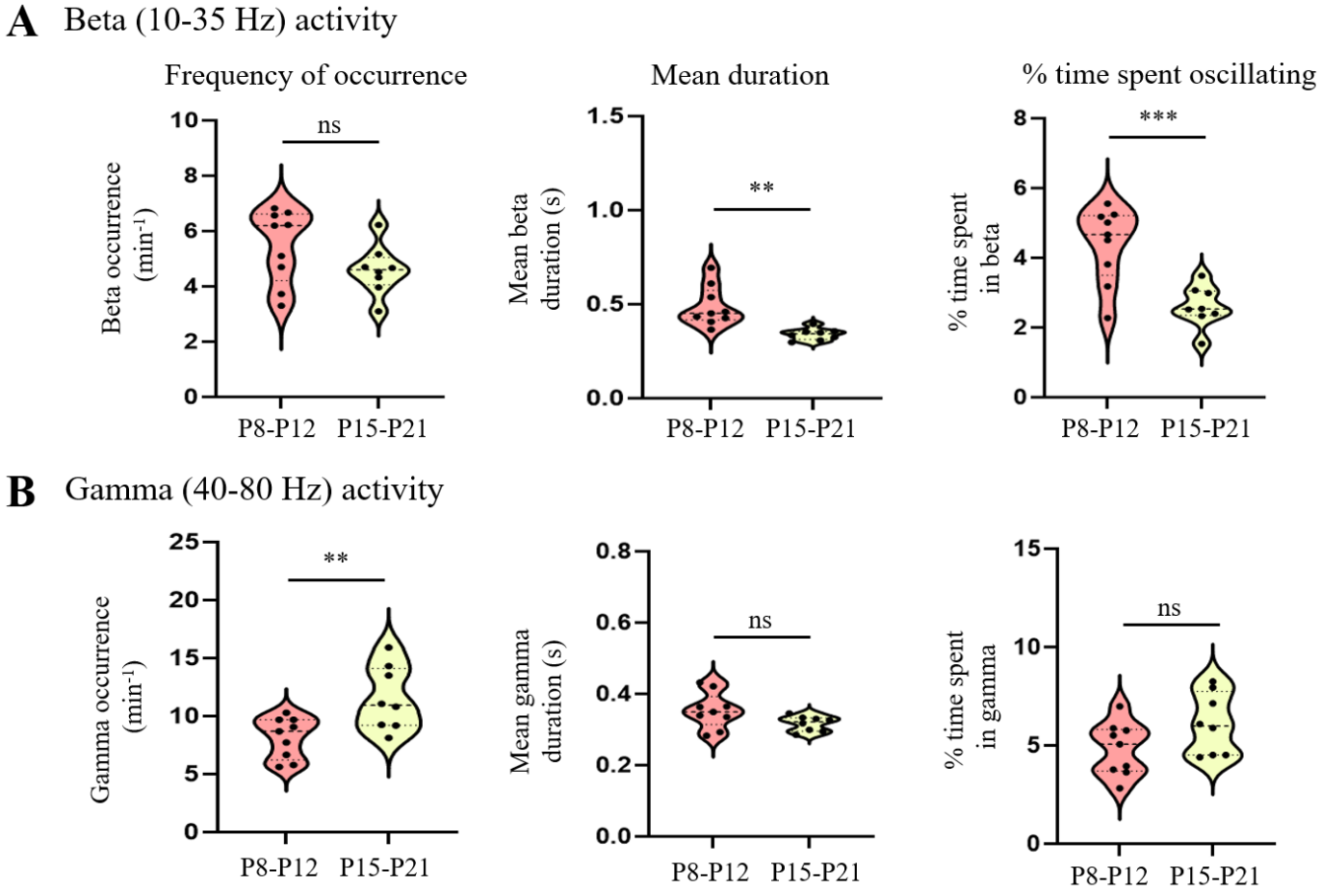


Figure 4: The effect of age on oscillatory activity during development. Violin plots indicating the frequency of occurrence, mean duration, and % time spent oscillating in beta (**A**) and gamma (**B**) in neonates (P8-P12) and juvenile (P15-P21) anaesthetised animals. Lines in the violin plots indicate the median and quartile values. Asterisks indicate significant difference between states (*p ≤ 0.05, ** p ≤ 0.01, and *** p ≤ 0.001), while ns indicates non-significance (p>0.05).

The decrease in the discontinuous spindle burst activity in the beta frequency range over development suggests that prefrontal beta activity is more critical earlier in development, gradually losing prominence after the onset of active sensory exploration (at P12). In contrast, this decline in beta activity is followed by an increase in gamma occurrence. Together this suggests that there is a timeline at which beta and gamma activity change their oscillatory characteristics and that, during development, the mPFC becomes gradually more able to support higher frequency activity.

3.2.3. Postnatal day 12 is a critical juncture in the development of oscillatory activity in the mPFC

To further explore the development of oscillatory activity, we next examined the percentage of time animals spend oscillating in either beta or gamma frequency on a day-by-day basis across the entire window recorded, from P8 to P21 (Figure 5A). This revealed that in the lead-up to P11, animals spent a similar amount of time oscillating in beta and gamma; from P11 to P12, there was a sudden drop in oscillatory activity across both frequency bands (beta: unpaired t-test $t(5) = 4.953$, $p = 0.0043$, gamma: unpaired t-test $t(5) = 3.291$, $p = 0.0217$, Figure 5B). After P12, the amount of time spent in beta and gamma activity decouples with beta decreasing and gamma frequency oscillatory activity increasing.

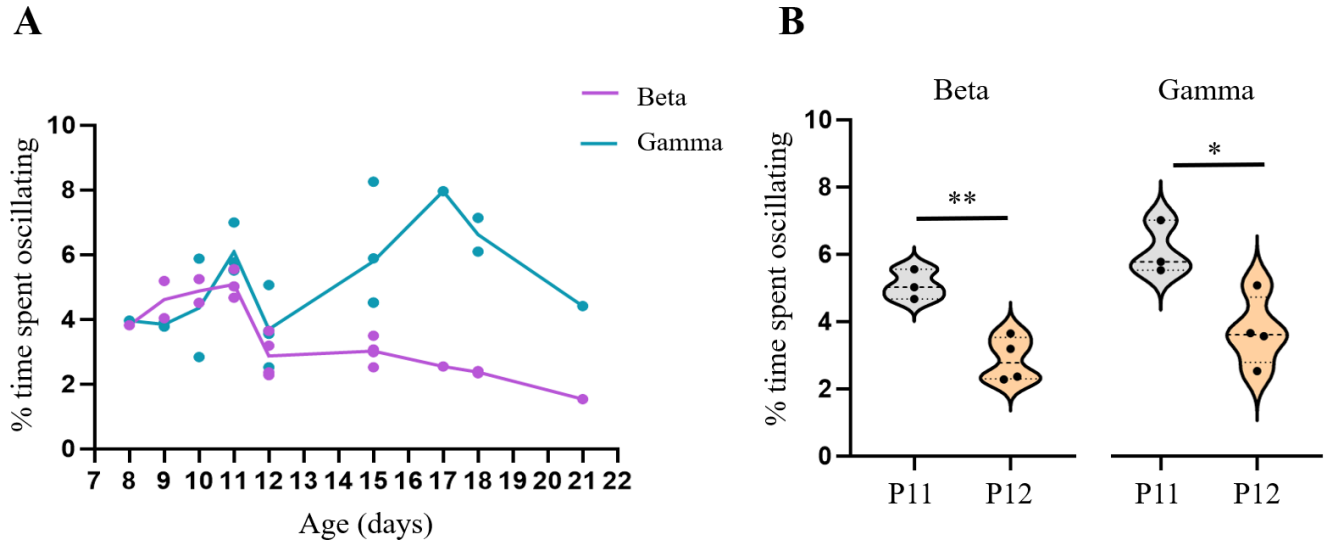


Figure 5: Beta and gamma oscillatory activity across development. A. Scatter plot of the percentages of time spent in either beta (magenta) or gamma (cyan) frequency range plotted for individual animals over development. The lines indicate the mean at each age. **B.** Percentage time spent oscillating in beta and gamma at P11 and P12 in anaesthetised animals. Lines in the violin plots indicate the median and quartile values. Asterisks indicate a significant difference between ages (*$p \leq 0.05$, ** $p \leq 0.01$).

This observation of a shift in neural activity at P12 matches observation in other cortices, primarily sensorimotor areas (Domínguez et al., 2021) and suggests a global shift in information transfer at this time in line with increased sensory awareness.

3.3. Single-unit activity across early postnatal development

We next focused on single-unit (SU) activity over the same developmental period. Raw data was sorted (Kilosort2, Pachitariu et al., 2016) and manually curated (see single-unit criteria in Methods) in Phy2 (Rossant et al., 2016) to identify single-unit activity. Single-units were then classified according to their spike waveforms. The shape of the spike, or its waveform, can be used to associate the spike with a particular neuronal cell type and a physiological state (Coleman and Burger, 2015). In total, we captured 600 single-units: 61 of those were captured in the awake, head-fixed neonates (P8-P12, N=3), 217 in the anaesthetised neonate (P8-P12, N=9), and the remaining 322 in the anaesthetised juvenile (P15-P21, N=8) animals (Figure 6A,B,C,D).

We first analysed trough-to-peak time versus half-width (Figure 6A) for each spike waveform to see if we could identify fast-spiking (FS) versus regular-spiking (RS) units early in development; fast-spiking units were classified by a cut-off of spike trough-to-peak time shorter than 0.75 milliseconds. Using this criterion, we captured 37 FS units, of which 1 was recorded in an anaesthetised neonate, 2 were recorded in awake neonates, and 34 were recorded in anaesthetised juveniles (Figure 6B, C, D, E). Unit half-widths were significantly larger (unpaired t-test: $t(276) = 4.459$, $p<0.0001$) in anaesthetised animals compared to awake animals (Figure 6F).

Unsurprisingly given the delayed maturation of FS intrinsic electrophysiological properties (Bitzenhofer et al., 2020), clear separation between FS and RS units was only unequivocally observed at later ages (post-P15) (Figure 6D). Larger half-width times are generally associated with more immature spike waveforms (Bitzenhofer et al., 2020), and it is conceivable that urethane affects the rectification of the action potential and thus gives single-units a more immature waveform (Figure 6F). This suggests that urethane affects not only populations of neurons but also individual neurons through modulating their spike waveforms.

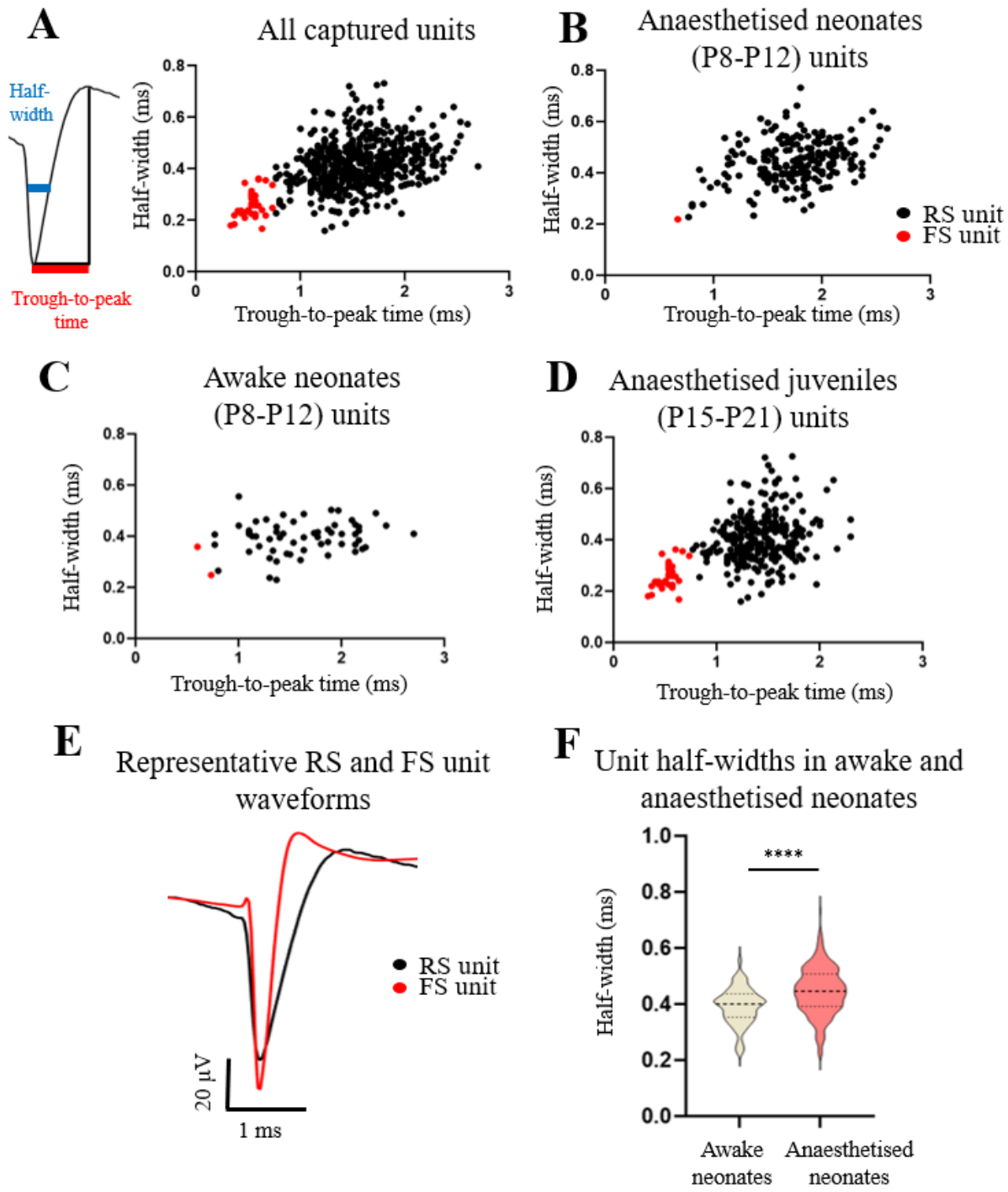


Figure 6: Single-unit waveform analysis. A. (left panel) Schematic indicating classical spike waveform features used in waveform analysis (trough-to-peak time (red) and half-width (blue); (right panel) scatter plots of spike trough-to-peak vs. half-widths for all recorded units. (**B**) SUs recorded in anaesthetised neonates, (**C**) awake neonates, and (**D**) anaesthetised juvenile animals. Black dots indicate regular-spiking (RS) units, and red dots indicate putative fast-spiking (FS) units with a 0.75 ms trough-to-peak time cut-off. **E.** Representative RS and FS spike waveforms. **F.** Plot of SU half-widths in awake and anaesthetised neonates (P8-P12). Lines in the violin plots indicate the median and quartile values. Asterisks indicate a significant difference between states (**** $p \leq 0.0001$).

A clear separation between FS and RS units observed at later ages (Figure 6B,C,D) was further corroborated when individual trough-to-peak latencies were examined by age (Figure 7A,B,C). A simple linear regression model of single-unit trough-to-peak latencies shows a significant correlation with age (n=600, $F(1,598) = 184.6$, $R^2 = 0.2359$, $p < 0.0001$) (Figure 7A). The ability to detect single-unit activity seemed to increase with age (Figure 7D); however, this effect was insignificant (unpaired t-test:$t(15) = 2.047$, $p = 0.0586$, Figure 7E). Finally, urethane anaesthesia did not alter our ability to detect single-units (unpaired t-test: $t(10) = 0.3626$, $p = 0.7244$, Figure 7F).

To investigate whether urethane anaesthesia and age differentially affect the ability to detect FS units compared to all units and to determine if the previously reported (Bitzenhofer et al., 2020) developmental gradient in intrinsic properties (translating to spike waveform properties) of FS units is present in our dataset, we analysed the numbers of detected FS units across all conditions. The proportion of FS units within all captured units increased during development (Figure 7G,H), with the first FS units appearing at P11. Furthermore, the number of FS units significantly increased at later ages (Mann-Whitney test: $U=5.0$, $p = 0.0008$).

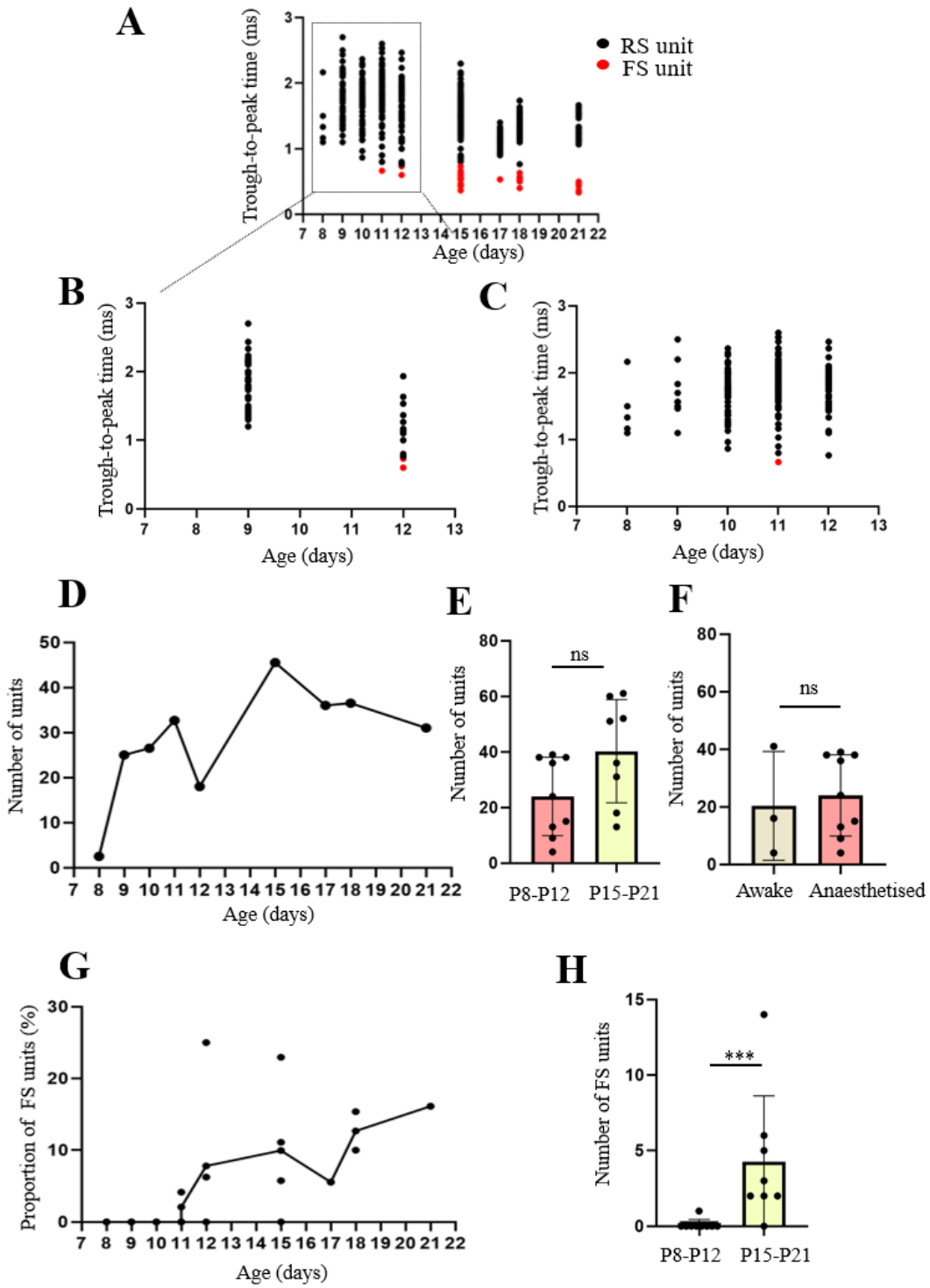


Figure 7: Single-unit properties through development and under anaesthesia. A. Scatter plots of spike trough-to-peak vs. age obtained from all animals, broken down by (**B**) awake and (**C**) anaesthetised neonates (P8-P12). Black dots indicate regular-spiking (RS) units, and red dots indicate fast-spiking (FS) units with a 0.75 ms trough-to-peak time cut off. **D.** Mean number of units per animal recorded at each age. **E & F.** The number of units (individual dots) obtained per animal +/- SD according to (**E**) age and (**F**) state. **G.** The proportions of FS units as a percentage of all units. The line represents the mean at each age. **H.** The number of FS units recorded across developmental time points. Asterisks indicate a significant difference between states (*** $p \leq 0.001$), while ns indicates non-significance ($p>0.05$).

3.3.1. Optogenetic tagging of *Nkx2-1*-derived interneurons in early postnatal mPFC

To identify putative SST+ and PV+ interneurons in the dataset and provide, we paired acute extracellular recordings with optical stimulation of PV+ and SST+ interneurons using an optoelectrode (Figure 1B).

We used *Nkx2-1-Cre:Ai32(ChR2)* pups to conditionally label *Nkx2-1*-derived cortical GABAergic interneurons in mPFC with *Channelrhodopsin2* (ChR2). This allows us to use blue light (473 nm) to optogenetic "tag" interneurons during early postnatal life. *Nkx2-1*-derived interneurons included the majority of PV+ and SST+ interneuron subtypes and therefore permitted the classification of these subtypes through early life when mature spike properties are absent (Kvitsiani et al., 2013), Blue light stimulation (20mW, 100 trial of 50 ms pulses with a 10-second inter-trial interval) elicited action potentials in ChR2-expressing interneurons along with inhibition of other RS units recorded on the same probe. To determine whether the response to stimulation is statistically significant, an analysis of variance (ANOVA) or Kruskal-Wallis test (for normal and non-normal distribution of spikes) was used to compare the baseline number of spikes (50 ms pre-stimulation) with the number of spikes in the 50 ms stimulation window (p-value, $p<0.05$). Although other approaches exist for the determination of statistical significance in optogenetic tagging experiments, this approach was deemed optimal for two reasons: (1) since we are activating GABAergic interneurons, this could, if these cells are inhibitory, lead to reduced firing in other neurons and (2) low reliability and delayed onset of ChR2 light-evoked spikes during early development necessitate the use of a prolonged stimulation window (50 ms).

Out of 600 single-units across all animals, 5 units significantly increased their firing rates during blue light stimulation (Figure 8). Three of those cells (U133, U140, U249) were from a urethane anaesthetised animal at P15, one (U239) was from a urethane anaesthetised animal at P11, and one (U235) was from a urethane anaesthetised animal at P18 (Figure 8A). In addition, raster plots indicate that significantly tagged units show a fairly unreliable response to blue light stimulation (Figure 8A) and peri-stimulus time histograms show an increase in their firing rates during blue light stimulation (Figure 8B).

Since the *Nkx2-1* line conditionally labels a number of populations of interneurons, we sought to identify putative PV+ interneurons based on spike waveform features of the tagged cells. Using the same classification described above, we identified that of the five optotagged units, four are regular spiking (U133, U249, U239, U235), and one is a fast-spiking (U140) unit (Figure 8C). The 4 regular spiking cells are likely SST+ interneurons, which play a prominent role in early development.

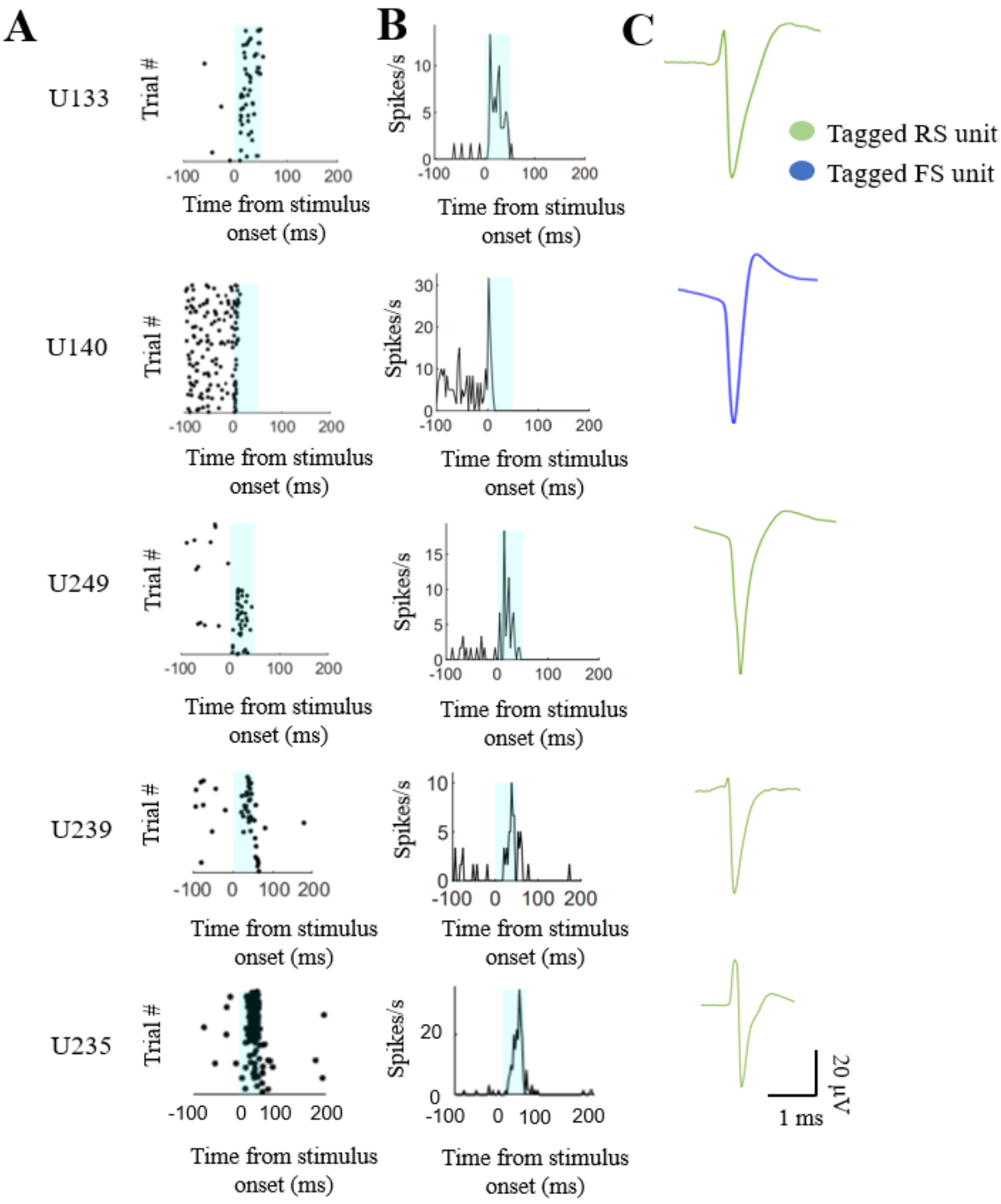


Figure 8: Optogenetic spike tagging of *Nkx2-1*-derived interneurons. A. Individual unit IDs and spike raster plots of single-units from *Nkx2-1-Cre:Ai32* transgenic mice showing spiking activity during blue light stimulation. **B.** Peri-stimulus time histograms (PSTH) for single-units that respond to blue light stimulation. **C.** Representative spike waveforms of tagged single-units. Green denotes RS, putative SST+ interneurons, and blue denotes the identified *Nkx2-1*-derived fast-spiking (FS) single-unit.

Since mature FS cells express PV+ (Bitzenhofer et al., 2020), and to harmonise nomenclature with identified RS tagged units, likely putative SST+ interneurons, we have distinguished them based on cardinal labels: PV+ and SST+ interneurons (Figure 9A,B).

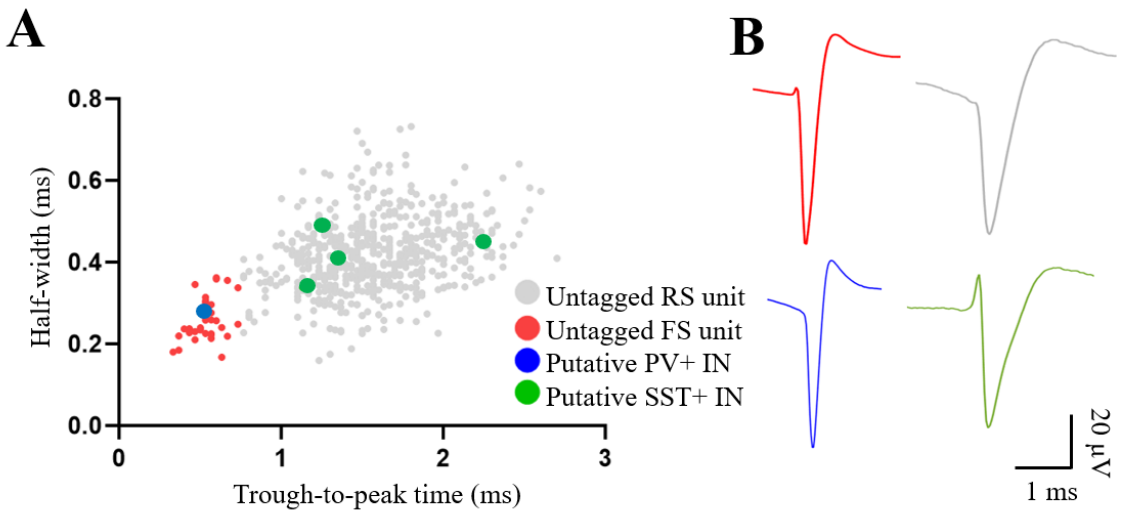
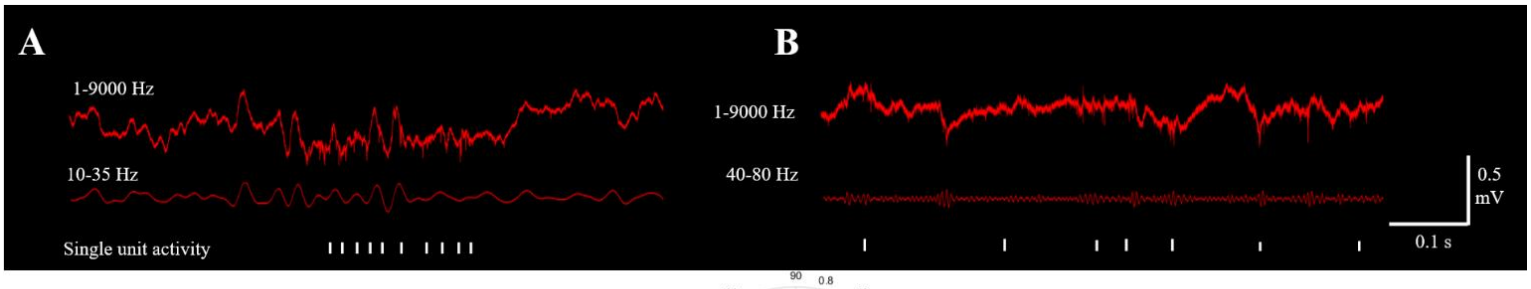
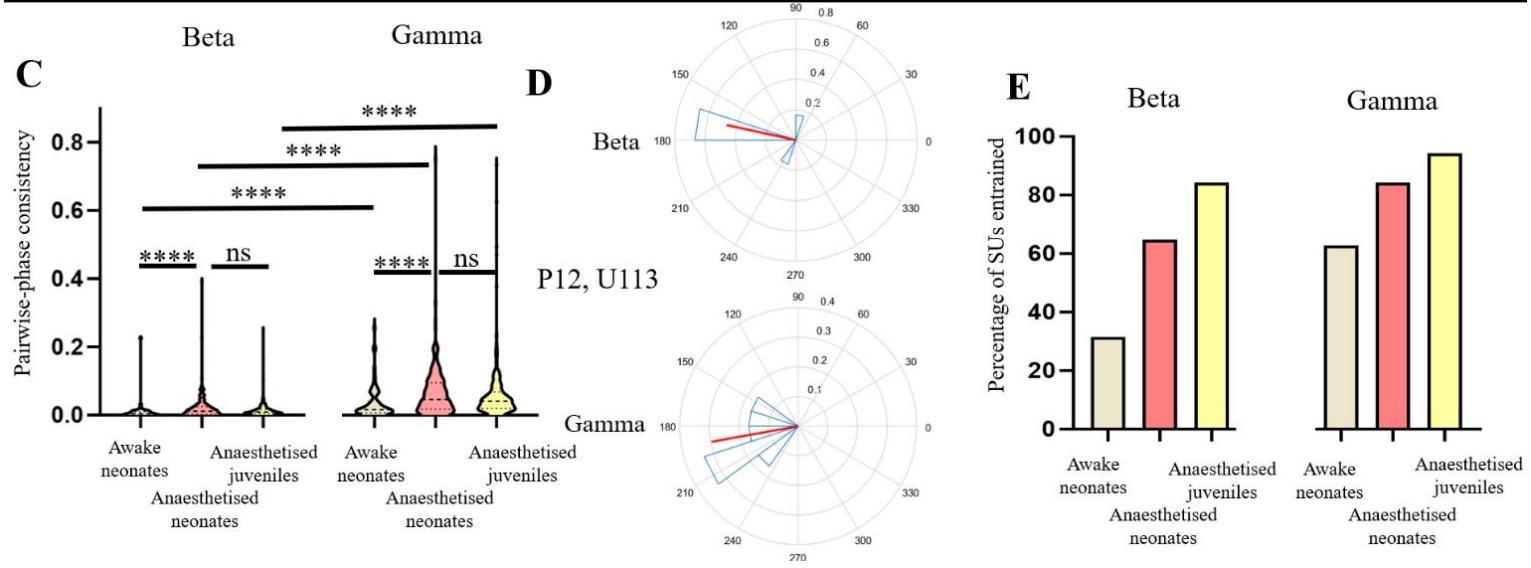


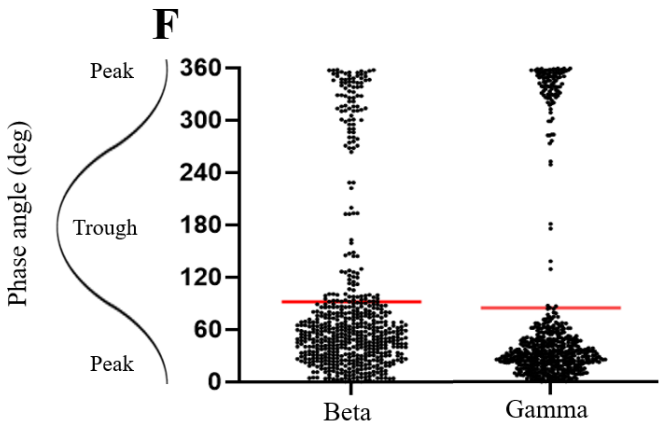
Figure 9: Identification of putative PV+ and putative SST+ interneurons within the *Nkx2-1* cohort. A. Spike trough-to-peak times vs. half-widths for all captured units with tagged *Nkx2-1* units highlighted; grey dots indicate untagged RS units, red indicate untagged FS units while blue and green denote putative PV+ interneurons (INs, tagged FS units) and putative SST+ interneurons (tagged RS units), respectively. **B.** Representative spike waveforms of all captured unit types. The colour scheme is the same as in panel A.

3.4. Spike-LFP entrainment analysis

Having characterised beta and gamma oscillatory activity under anaesthesia through postnatal development and then examined the properties of optotagged and other single-units, we now examined if single-units are entrained by beta and gamma network oscillations.
To analyse this, we examined the temporal correlation between the individual single-unit spikes in relationship to the LFP. LFPs were captured and bandpass filtered in the beta and gamma frequency ranges and the timings of single-unit spikes were recorded (Figure 10A, B). To determine the strength of entrainment of a given single-unit, we computed the pairwise-phase consistency (PPC) value for every unit in beta and gamma frequency ranges. As such, the PPC estimates the similarity of the relative phase observed in one spike trial to the relative phase observed in another spike trial (Vinck et al., 2010).
To examine the spike-LFP-coupling during development and under anaesthesia, we compared the PPC values of all captured units across groups of animals and different oscillation frequency ranges (Figure 10C).
Urethane anaesthesia significantly increased the strength of unit entrainment for both beta (Kruskal Wallis test: X^2=25.94, p<0.0001) and gamma (Kruskal Wallis test: X^2=25.94, p<0.0001) oscillations. However, the level of entrainment in beta or gamma does not change over development (Kruskal Wallis test, X^2=25.94 p>0.99).
On average, across all units, gamma frequency oscillations entrain units more strongly than during beta frequency across all groups of animals (awake neonates (Wilcoxon matched-pairs signed rank test: W=1479, p<0.0001), anaesthetised neonates (Wilcoxon matched-pairs signed rank test: W=18688, p<0.0001) and anaesthetised juveniles (Wilcoxon matched-pairs signed rank test: W=50733, p<0.0001), Figure 10C).
Additionally, the percentage of units significantly entrained (Figure 10D) in beta frequency oscillations is higher in anaesthetised neonates (64.6%) than in awake neonates (31.5%) and in anaesthetised juveniles (84.2%) compared to anaesthetised neonates (64.6%). The same is true for gamma frequency; the percentage of units significantly entrained is higher in anaesthetised neonates (84.3%) than in awake neonates (62.7%) and in anaesthetised juvenile animals (94.1%) compared to anaesthetised neonates (62.7%) (Figure 10E). We also examined the peak phase at which single-units fire and found that single-unit activity is entrained more sharply to the peak of gamma frequency activity than during beta frequency oscillations (Figure 10F).
After examining the overall entrainment of all units across groups, we then broke the data down by unit subtype because neurons have been shown to respond to different frequencies present in their synaptic input in different ways, which results in the preferential phasic firing of some neuronal types (Oren et al., 2006). RS and FS units were not differentially entrained in beta (Mann-Whitney test: U=8450, p = 0.0761) nor gamma (Mann-Whitney test: U=8907, p = 0.1882) (Figure 10G, H) frequency oscillations.
Taken together, these data indicate that urethane anaesthesia increases the strength of unit entrainment for both beta and gamma oscillations in the mPFC of juvenile animals (<P21). In addition, gamma frequency activity entrains more units (Figure 10E) more strongly (Figure 10C) and more precisely than beta frequency oscillations (Figure 10F), suggesting that gamma frequency activity has a more prominent effect in synchronising single-unit activity than beta - even at early ages – prior to P21.


A
1-9000 Hz
10-35 Hz
Single unit activity
B
1-9000 Hz
40-80 Hz
0.5 mV
0.1 s


Beta
Gamma
C
Pairwise-phase consistency
****
****
****
****
ns
****
ns
Awake neonates
Anaesthetised juveniles
Anaesthetised neonates
Awake neonates
Anaesthetised juveniles
Anaesthetised neonates
D
Beta
P12, U113
Gamma
E
Beta
Gamma
Percentage of SUs entrained
Awake neonates
Anaesthetised juveniles
Anaesthetised neonates
Awake neonates
Anaesthetised juveniles
Anaesthetised neonates


F
Peak
Trough
Peak
Phase angle (deg)
Beta
Gamma

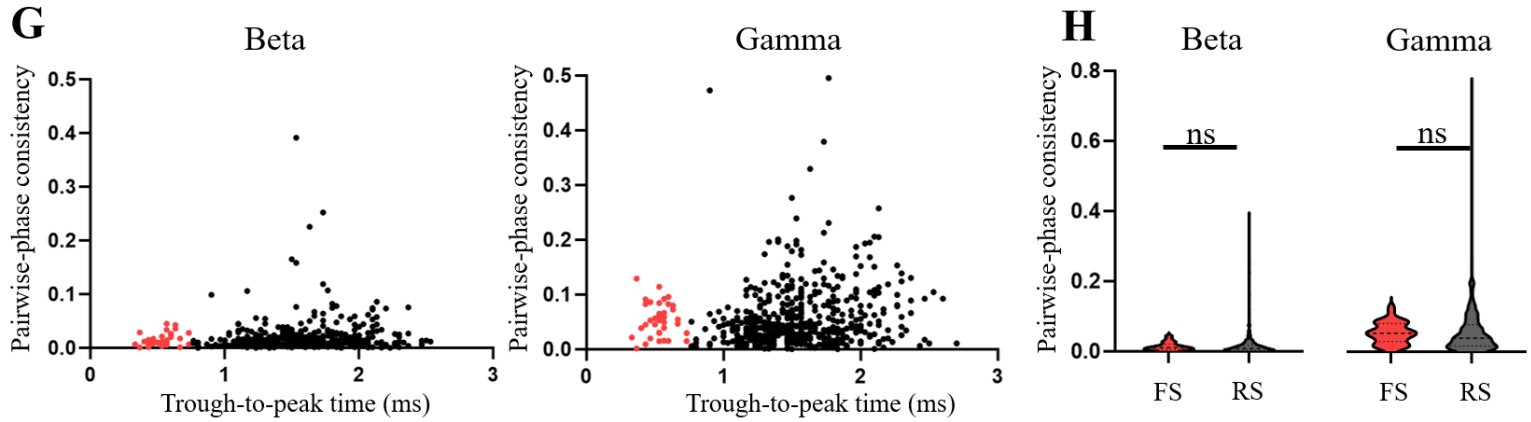

G
Beta
Gamma
Pairwise-phase consistency
Trough-to-peak time (ms)
Trough-to-peak time (ms)
H
Beta
Gamma
ns
ns
FS
RS
FS
RS

Figure 10: Unit entrainment in beta and gamma oscillations. Representative extracellular recordings of LFP (1-9000 Hz, **AB**), beta (10-35 Hz, **A**), and gamma activity (40-80 Hz, **B**) after bandpass filtering. White lines indicate the timing of single-unit activity in relation to the LFP. **C.** Pairwise-phase consistency (PPC) values for single-units captured in each group of animals during beta and gamma frequency oscillation. Asterisks indicate a significant difference between groups following *post-hoc* analysis corrected for multiple comparisons (Dunn's test); ****$p<0.0001$. **D.** Polar histogram plot of a significantly entrained single-unit (U113, Raleigh test of circular uniformity, $p<0.05$) recorded from a P12 urethane-anaesthetised animal; red line, mean vector of the histogram. **E.** The ratio of all captured units in each group significantly entrained by both beta and gamma frequency oscillations. Significance was measured by the Raleigh test for non-uniformity (significance is set at $p<0.05$). **F.** The phase values of all captured units in beta and gamma frequency oscillations of a bandpass filtered signal. The trough of the oscillation is set at 180°, and 0° and 360° are set as the peak of the oscillation. The red line indicates the mean phase value for each oscillation type. Across all panels, lines in the violin plots indicate the median and quartile values. Asterisks indicate a significant difference (*=$p<0.05$), while ns indicates non-significance ($p>0.05$). **G.** Relationship between the strength of entrainment (PPC) in beta and gamma frequency oscillations and the trough-to-peak time of individual single-units. Dots indicate a single-unit (red, FS; black, RS). **H.** The strength of entrainment (PPC) in beta and gamma frequency oscillations between all FS and RS units.

3.4.1. Contribution of putative PV+ and SST+ interneurons to beta and gamma frequency oscillations

We next examined the contribution of putative GABAergic interneurons to oscillatory activity during early development. We recorded 5 optotagged *Nkx2-1* interneurons (1 putative PV+ and 4 putative SST+ interneurons) and 37 untagged FS units identified on waveform alone. All FS units are classified as putative PV+ interneurons, according to Bitzenhofer et al., 2020.

Both putative interneuron subtypes show entrainment in beta and gamma oscillations across the development, with entrainment in gamma more pronounced when compared to the beta frequency band (Figure 11A). Within beta frequency oscillations, putative PV+ interneurons are more strongly entrained than the small number of putative SST+ interneurons (Mann-Whitney test: $U=19$, $p = 0.012$). However, this effect is not observed in the gamma frequency band (Mann-Whitney test: $U=38$, $p = 0.1218$) (Figure 11B), where both interneuron populations show a similar degree of entrainment. This suggests that even though gamma activity is increasing over development, the putative SST+ and PV+ interneuron subtypes respond to changing gamma similarly.

PPC is computed throughout the entire baseline of the filtered LFP and, as such, includes spikes outside of beta or gamma events, potentially diminishing the calculated contribution of the unit to these events. To address this concern, we tested another method of analysis - the inter-spike interval (ISI) shuffle method (Narayanan and Laubach, 2009). This method involves predefining oscillatory events and computing the ratio of spikes firing within just these events to the total spike counts for a given unit (Figure 11C). A unit was classified as entrained by an oscillatory event if the real spike probability was greater in at least 99.9% of cases. The spike probabilities of the 5 optically tagged interneurons in defined beta or gamma frequency events are shown in Figure 11D.

This analysis revealed that across all single-units from P11 to P18, putative SST+ interneurons and the single recorded *Nkx2-1*-derived putative PV+ interneuron fire significantly more spikes during beta and gamma frequency oscillations when compared to baseline. There is also a suggestion of decoupling between SST+ interneuron entrainment in beta and gamma frequency oscillations post P12. This mirrors our previous observation at the population level (Figure 5A).

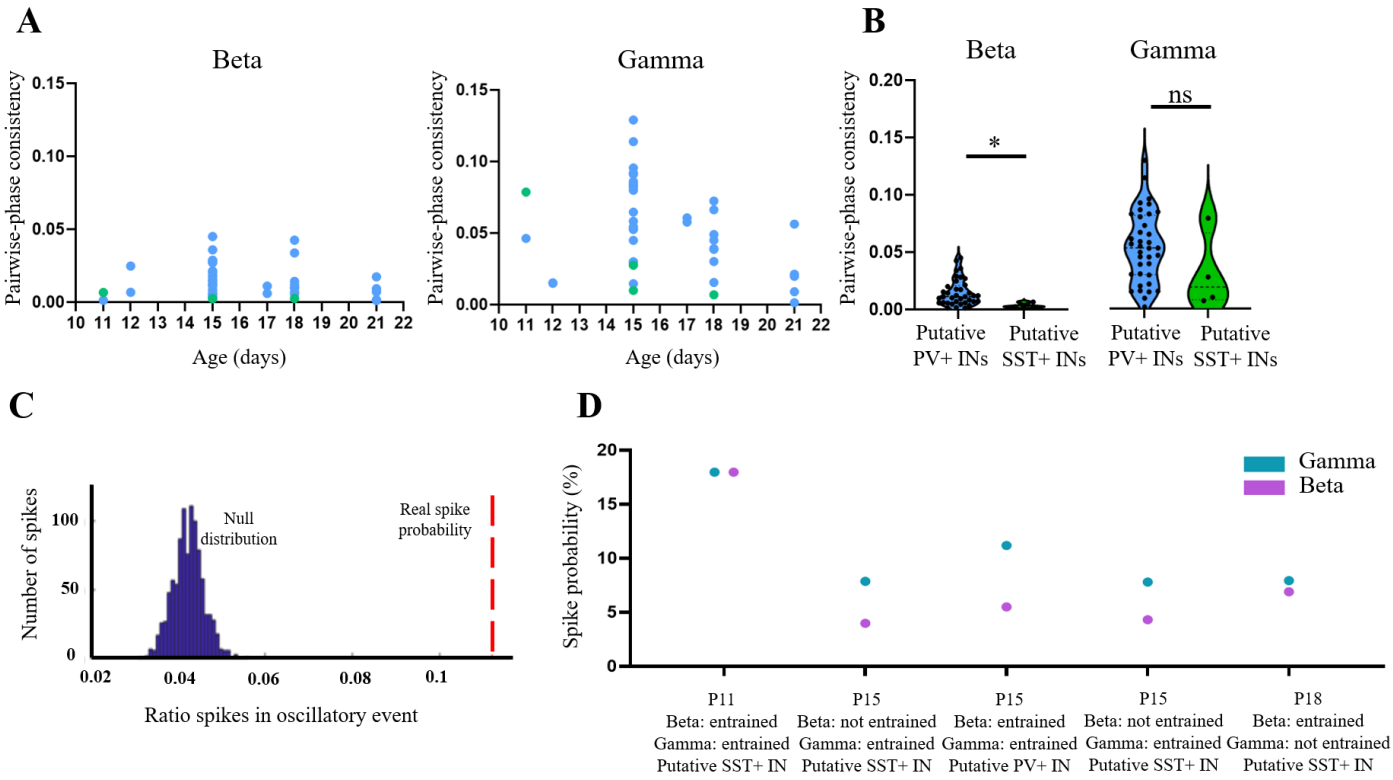


Figure 11: Involvement of putative GABAergic interneuron subtypes in beta and gamma frequency oscillations during development. A. PPC of putative GABAergic interneuron subtypes in beta and gamma frequency oscillations through development. Dots indicate a single putative GABAergic interneuron unit (blue, putative PV+ interneuron; green, putative SST+ interneuron). **B.** The strength of entrainment (PPC) in beta and gamma frequency oscillations between all putative PV+ interneurons (INs) and putative SST+ interneurons; black dots indicate individual PPC values of individual units. **C.** Inter-spike interval shuffling method of determining single-unit spike firing within oscillatory events. An example histogram plot indicates the shuffled inter-spike intervals for a single-unit, and the red line indicates the real probability of a spike to occur within an oscillatory event. To statistically examine the significance of single-unit firing in beta and gamma oscillations, inter-spike intervals of a single-unit were permuted and shuffled 1000 times to create the null distribution (blue histogram). The probability of spikes occurring in a beta or gamma event was calculated as the ratio between the number of spikes occurring within defined beta or gamma events over the total number of spikes during the baseline recording. **D.** Spike probabilities and entrainment of optotagged interneurons. Dots indicate the individual spike probabilities for each optotagged unit in beta (magenta) and gamma (cyan) oscillations. Lines in the violin plots indicate the median and quartile values. Asterisks indicate a significant difference between states (*=$p<0.05$), while ns indicates non-significance ($p>0.05$).

4. DISCUSSION

In this study, we examined the early postnatal activity in the developing mPFC. Specifically, (1) we characterised the features of early beta and gamma frequency oscillatory events both under anaesthesia and in head-fixed mice during development, (2) we characterised the development of single unit activity and identified putative PV+ and SST+ interneurons in the dataset, and (3) we examined how single units and putative PV+ and SST+ interneurons contribute to beta and gamma frequency activity during development.

Oscillations in the beta (10-35 Hz) and gamma (40-80 Hz) frequency ranges underpin the functional development of the mPFC (Chini and Hanganu-Opatz, 2021). Spindle bursts - thalamocortical oscillations in the beta frequency range occurring across the developing neocortex, are observed in the developing mPFC until P12, after which they become more infrequent and eventually difficult to detect (Gomez et al., 2022). In contrast, gamma activity shows a pronounced increase in frequency and amplitude from the second postnatal week and further during development (Bitzenhofer et al., 2020).

In this study, we detected both beta and gamma activity at all recorded ages (P8-P21). However, bursts of beta activity became shorter, and gamma frequency oscillations occurred more frequently with age. In addition, we have shown that this divergence in activity patterns happens at P12 - preceded by a drop in overall beta and gamma activity. The differences in oscillations between the passive sensory (P8-P12) and active sensory (P15-P21) stages of development have been previously described; P12 is a time point at which prefrontal activity transitions from discontinuous to a continuous pattern (Chini et al., 2021). Additionally, we have found a significant drop in activity between P11 and P12 immediately preceding the decoupling of beta and gamma activity. This has been described in the developing somatosensory cortex, where it occurs at P9 (Domínguez et al., 2021).

While the physiological significance of this drop in activity and whether it induces the decoupling of beta and gamma activity are unclear, the mPFC circuits may be undergoing these dynamical changes in activity in order to support the incoming higher-order processing demands that come with the stage of active sensing in the period following P12 (eye and ear opening, active whisking, Martini et al., 2021). This supports the idea that, similar to primary sensory areas, P12 is a critical juncture in the maturation of the mPFC.

The impact of anaesthesia on postnatal cortical activity is poorly understood. Here, we have explored the impact of urethane anaesthesia – commonly used in studies on primary sensory areas in neonates (Minlebaev et al., 2011), affects the spontaneous occurrence of beta oscillations. Urethane is a common anaesthetic in rodent developmental neurophysiological experiments as it preserves information processing in developing sensory cortices (Chini et al., 2019, Shumkova et al., 2021). While its mechanisms of action at the single neuron and population level are still relatively unknown, urethane has a frequency-unspecific dampening effect on neuronal activity in the developing mPFC (Chini et al., 2019).

Here, we have found that urethane significantly increases the occurrence of beta frequency events and does not affect gamma activity pre-P12. As early beta frequency activity is driven by the thalamus (Minlebaev et al., 2007), this may indicate a urethane-induced increased thalamic drive into the mPFC at this age. However, this result is surprising as urethane has been reported to reduce the rate of spindle bursts in the developing mPFC pre-P12 (Gomez et al., 2022). This may be due to a different definition of beta oscillation/spindle burst (we used 10-35 Hz, Gomez et al. used 10-20 Hz) or a different anaesthetic protocol (sequential intraperitoneal injections over 1 hour before recording/subcutaneous infusion through a cannula during recording).

Together, this may suggest that urethane anaesthesia differentially affects beta oscillations and spindle bursts and that urethane administration protocol may modulate urethane's effect on oscillations in the beta frequency range.

Further, while it is clear that urethane anaesthesia has pronounced effects on the population activity (LFP) throughout development, the effects of urethane on the activity of single neurons are less understood. Here, we report a significant increase in unit half widths as an effect of urethane anaesthesia on the mPFC pre-P12. Interestingly, this effect of urethane has not been previously detected, and in the adult rat visual cortex, urethane has been reported to depress neuronal excitability but not affect single neuron half-widths (Sceniak and MacIver, 2005). Our data suggest that urethane anaesthesia alters spike kinetics as well as the broad population activity of developing neurons in the mPFC.

In the adult cortex, FS interneurons underpin gamma frequency oscillations (Cardin et al., 2009). In developing mPFC, FS interneuron maturation patterns correlate with the emergence and strengthening of gamma activity (Bitzenhofer et al., 2020). Here, we examined the timeline of the maturation of FS interneurons and gamma oscillatory activity. FS interneurons were first detected based on spike waveform at P11, consistent with previous studies (Bitzenhofer et al., 2020) and broadly consistent with the increased prominence of gamma from P12 onward.

However, we have also detected fast oscillatory activity in the gamma range earlier than P11 - suggesting that gamma activity is present when FS interneurons have not yet acquired their fast-spiking phenotype. Instead, they show an immature spike waveform indistinguishable from regular-spiking units.

This suggests two possible mechanisms of early gamma oscillations in the developing mPFC: (1) a mechanism relying on chemical synaptic transmission independent of fast-spiking spike kinetics of interneurons – possibly early gamma oscillations originate from the feedforward gamma-rhythmic excitatory input from the thalamus - as observed in the developing somatosensory cortex (Khazipov et al., 2013). (2) A mechanism of early gamma oscillations entirely independent of chemical transmission - one possibly involving gap junctions. Gap junction channels connect the cytosol of two neighbouring neurons and allow for the exchange of ion channels - essentially enabling a fast and low resistance means of electrical coupling between two neurons (Niculescu and Lohmann, 2014). The gap junctions would provide a rapid means of correlating cell-to-cell activity; however, they would not correlate them in any particular frequency band – that would likely involve an interplay between local excitatory and inhibitory neurons.

During early postnatal cortical development, specifically the first postnatal week, gap junctions have been implicated in synchronising bursts of beta activity across sensory areas (Hanganu et al., 2006, Dupont et al., 2005). However, due to the protracted development of the mPFC in relation to sensory areas (Caballero et al., 2016), it is possible that the gap junction mechanism of transmission may extend up to the emergence of the fast-spiking phenotype of neurons in the second postnatal week and may extend to enable fast oscillatory activity.

To identify putative PV+ and SST+ interneurons, we conditionally expressed *Channelrhodopsin2* in *Nkx2-1*-derived cortical interneurons (Xu et al., 2008). Out of 600 single units, we have only identified five tagged *Nkx2-1* neurons. This is surprising because the same strategy has previously proven successful in optotagging and identifying interneurons in developing primary somatosensory and visual cortex (Ghezzi et al., unpublished). One possible reason for the low optotagging yield could be that the orientation of cortical layers in the mPFC differs from primary sensory areas, and the penetration of the optoelectrode is likely within a single mPFC layer rather than across layers throughout the depth of primary sensory areas. The higher density of *Nkx2-1* interneurons in deeper layers of the primary sensory cortices could result in a reduced sampling of these units (Anastasiades and Marques-Smith et al., 2016). Histological characterisation of the distribution of *Nkx2-1*-derived interneurons in mPFC is pending (Pilli & Butt, unpublished data) and could provide further insight into the ideal stereotaxic coordinates to target these interneurons in future recordings. A further reason could be that the developmental time course of the *Nkx2-1* transgenic line is different from wild-type and that channelrhodopsin is insufficiently expressed or ineffectively trafficked to neuronal membranes at the here-examined time points.

Understanding neural activity requires information both at the level of neural circuits and single neurons (Yuste, 2008). The activity of single neurons and populations of neurons is closely related, and some neuronal types show preferential entrainment to specific frequency ranges (Wilson et al., 2018) – which reflects involvement in that frequency range. Here, we investigated the degree of spike-LFP synchrony in the developing mPFC for different single units and putative GABAergic interneurons in beta and gamma frequency oscillations. Additionally, we examined the effects of urethane anaesthesia on spike-LFP synchrony in animals younger than P12. We found that urethane anaesthesia increased the strength of entrainment of all units in neonatal animals. Recently it has been shown that anaesthesia has a prominent role in synchronising cortical activity in a layer-specific manner in adults (Bharioke et al., 2022). This suggests that (1) urethane has similar synchronising effects on cortical networks as other anaesthetics (isofluorane and ketamine, Bharioke et al., 2022) and (2) even immature networks in the mPFC can respond to urethane. This may indicate that anaesthetic effects on neural synchrony are independent of the maturation stage of neuronal populations.

Further, we also found that the maturation of neural circuits did not alter the degree of spike-LFP synchrony for beta nor gamma frequency oscillations - indicating that as oscillations change their features through development, the degree of entrainment of single neurons in those oscillatory events does not change. While this may be true for the developing mPFC, other cortical areas have different maturational patterns (Choi, 2018), and it remains to be seen how the degree of unit synchrony varies during the development of different cortical areas.

Comparing beta and gamma frequency oscillations, we have shown that gamma activity has a more substantial effect in involving single unit activity than beta, independent of age or anaesthesia. Single-unit involvement in gamma activity represents a form of synchrony often influenced and induced by cognitive and behavioural states (Kohn et al., 2009).

In the early visual cortex of primates, it has been shown that unit synchrony within gamma frequency oscillations is dependent on sensory input (Jia et al., 2013). While the developing murine mPFC activity is modulated by behavioural state (Gomez et al., 2022), it is unclear if it processes sensory information early in development - and it is unclear what the role of gamma unit synchrony is early in mPFC development, especially in anaesthetised animals.

Furthermore, we broke down the single units by type and examined their entrainment strengths in beta and gamma frequency oscillations during mPFC development. We showed that while FS units (putative PV+ interneurons) do not differ in their beta and gamma frequency entrainment from RS units (putative excitatory neurons), they show stronger entrainment in beta frequency oscillations compared to optotagged putative SST+ interneurons prior to P21.

Because neuronal subtypes engage differentially in cortical circuits, they are recruited and engaged in synchrony across different frequency bands in adult animals (Wilson et al., 2018). This appears to be the case in mPFC development, particularly in the case of developing putative PV+ and SST+ interneurons. To examine at which stage this differential spike-LFP coupling occurs, we examined the optotagged interneurons more accurately according to their spike probabilities in beta and gamma frequency events. We observed a similar decoupling pattern between P11 and P15 for both beta and gamma frequency activity - further corroborating our previous finding that a critical period for the maturation of prefrontal networks occurs around P12. This supports the notion that this critical juncture likely reflects shifts in the circuit roles of PV+ and SST+ interneurons in mPFC.

Local interneuron networks in the mPFC show a wide range of reciprocal interactions with oscillatory activity in adult animals (Ferguson and Gao, 2018, Abbas et al., 2018). Here, we suggest that this complex synchrony between local PV+, SST+ interneurons, and global oscillatory activity is important in the development of the mPFC with a possible critical period around P12. Understanding spike-LFP synchrony during the development of the mPFC is critical as deficits in these interactions have been hypothesised to underpin neurodevelopmental disorders such as autism and schizophrenia (Chattopadhyaya and Di Cristo, 2012).

This work represents one year of training and data analysis. In many ways, it is far from complete, but it does give us further insight into when to look for circuits and systems-level changes. Future experiments could focus on characterising the local circuitry in the developing mPFC to examine whether activity recorded *in vivo* is underpinned by a shift in the make-up and nature of local circuits. Specifically, it would be interesting to know if the connectivity and spatial distribution of GABAergic interneuron populations change over development in line with our *in vivo* observations. Together, our *in vivo* and future *in vitro* experiments will provide a detailed assessment of the developing murine mPFC with a focus on GABAergic interneurons.

While PFC-mediated behaviours and activity at the adult stage of development have become relatively well understood (Le Merre et al., 2021), the mechanisms underlying functional development and the emergence of neuronal activity have received less attention. Understanding the development of the PFC and, more specifically, how interneurons constrain emergent activity in this higher-order brain region is of interest to our further understanding of the aetiology of neurodevelopmental disorders.

References

Abbas AI, Sundiang MJM, Henoch B, et al. Somatostatin Interneurons Facilitate Hippocampal-Prefrontal Synchrony and Prefrontal Spatial Encoding. Neuron. 2018;100(4):926-939.e3. doi:10.1016/j.neuron.2018.09.029

Ackman JB, Burbridge TJ, Crair MC. Retinal waves coordinate patterned activity throughout the developing visual system. Nature. 2012;490(7419):219-225. doi:10.1038/nature11529

Ährlund-Richter S, Xuan Y, van Lunteren JA, et al. A whole-brain atlas of monosynaptic input targeting four different cell types in the medial prefrontal cortex of the mouse [published correction appears in Nat Neurosci. 2019 Apr 15;:]. Nat Neurosci. 2019;22(4):657-668. doi:10.1038/s41593-019-0354-y

American Psychiatric Association. Diagnostic and Statistical Manual of Mental Disorders (DSM-5) 5th ed. American Psychiatric Association; Washington, DC, USA: 2013.

Anastasiades PG, Carter AG. Circuit organization of the rodent medial prefrontal cortex. Trends Neurosci. 2021;44(7):550-563. doi:10.1016/j.tins.2021.03.006

Anastasiades PG, Marques-Smith A, Lyngholm D, et al. GABAergic interneurons form transient layer-specific circuits in early postnatal neocortex. Nat Commun. 2016;7:10584. Published 2016 Feb 4. doi:10.1038/ncomms10584

Atallah BV, Scanziani M. Instantaneous modulation of gamma oscillation frequency by balancing excitation with inhibition. Neuron. 2009;62(4):566-577. doi:10.1016/j.neuron.2009.04.027

Bharioke A, Munz M, Brignall A, et al. General anesthesia globally synchronizes activity selectively in layer 5 cortical pyramidal neurons. Neuron. 2022;110(12):2024-2040.e10. doi:10.1016/j.neuron.2022.03.032

Bissonette GB, Powell EM. Reversal learning and attentional set-shifting in mice. Neuropharmacology. 2012;62(3):1168-1174. doi:10.1016/j.neuropharm.2011.03.011

Bitzenhofer SH, Pöpplau JA, Hanganu-Opatz I. Gamma activity accelerates during prefrontal development. Elife. 2020;9:e56795. Published 2020 Nov 18. doi:10.7554/eLife.56795

Buzsáki G, Anastassiou CA, Koch C. The origin of extracellular fields and currents--EEG, ECoG, LFP and spikes. Nat Rev Neurosci. 2012;13(6):407-420. Published 2012 May 18. doi:10.1038/nrn3241

Buzsáki G, Draguhn A. Neuronal oscillations in cortical networks. Science. 2004;304(5679):1926-1929. doi:10.1126/science.1099745

Buzsáki G, Llinás R. Space and time in the brain. Science. 2017;358(6362):482-485. doi:10.1126/science.aan8869

Caballero A, Granberg R, Tseng KY. Mechanisms contributing to prefrontal cortex maturation during adolescence. Neurosci Biobehav Rev. 2016;70:4-12. doi:10.1016/j.neubiorev.2016.05.013

Cardin JA, Carlén M, Meletis K, et al. Driving fast-spiking cells induces gamma rhythm and controls sensory responses. Nature. 2009;459(7247):663-667. doi:10.1038/nature08002

Carmichael ST, Price JL. Connectional networks within the orbital and medial prefrontal cortex of macaque monkeys. J Comp Neurol. 1996;371(2):179-207. doi:10.1002/(SICI)1096-9861(19960722)371:2<179::AID-CNE1>3.0.CO;2-#

Chattopadhyaya B, Cristo GD. GABAergic circuit dysfunctions in neurodevelopmental disorders. Front Psychiatry. 2012;3:51. Published 2012 May 31. doi:10.3389/fpsyt.2012.00051

Chen G, Zhang Y, Li X, et al. Distinct Inhibitory Circuits Orchestrate Cortical beta and gamma Band Oscillations. Neuron. 2017;96(6):1403-1418.e6. doi:10.1016/j.neuron.2017.11.033

Chini M, Gretenkord S, Kostka JK, et al. Neural Correlates of Anesthesia in Newborn Mice and Humans. *Front Neural Circuits*. 2019;13:38. Published 2019 May 22. doi:10.3389/fncir.2019.00038

Chini M, Hanganu-Opatz IL. Prefrontal Cortex Development in Health and Disease: Lessons from Rodents and Humans. Trends Neurosci. 2021;44(3):227-240. doi:10.1016/j.tins.2020.10.017

Chini M, Pfeffer T, Hanganu-Opatz I. An increase of inhibition drives the developmental decorrelation of neural activity. Elife. 2022;11:e78811. doi:10.7554/eLife.78811

Cho KK, Hoch R, Lee AT, Patel T, Rubenstein JL, Sohal VS. Gamma rhythms link prefrontal interneuron dysfunction with cognitive inflexibility in Dlx5/6(+/-) mice. Neuron. 2015;85(6):1332-1343. doi:10.1016/j.neuron.2015.02.019

Choi, SY. Synaptic and circuit development of the primary sensory cortex. Exp Mol Med 50, 1–9 (2018). https://doi.org/10.1038/s12276-018-0029-x

Clarke HF, Dalley JW, Crofts HS, Robbins TW, Roberts AC. Cognitive inflexibility after prefrontal serotonin depletion. Science. 2004;304(5672):878-880. doi:10.1126/science.1094987

Clement EA, Richard A, Thwaites M, Ailon J, Peters S, Dickson CT. Cyclic and sleep-like spontaneous alternations of brain state under urethane anaesthesia. *PLoS One*. 2008;3(4):e2004. Published 2008 Apr 16. doi:10.1371/journal.pone.0002004

Cobb SR, Buhl EH, Halasy K, Paulsen O, Somogyi P. Synchronization of neuronal activity in hippocampus by individual GABAergic interneurons. Nature. 1995;378(6552):75-78. doi:10.1038/378075a0

Coleman, William L., and R. Michael Burger, 'Extracellular Single-Unit Recording and Neuropharmacological Methods', in Ellen Covey, and Matt Carter (eds), Basic Electrophysiological Methods (New York, 2015; online edn, Oxford Academic, 1 Apr. 2015), https://doi.org/10.1093/med/9780199939800.003.0003, accessed 6 Oct. 2022.

Colonnese M, Khazipov R. Spontaneous activity in developing sensory circuits: Implications for resting state fMRI. Neuroimage. 2012;62(4):2212-2221. doi:10.1016/j.neuroimage.2012.02.046

Domínguez S, Ma L, Yu H, et al. A transient postnatal quiescent period precedes emergence of mature cortical dynamics. Elife. 2021;10:e69011. Published 2021 Jul 23. doi:10.7554/eLife.69011

Ferguson BR, Gao WJ. PV Interneurons: Critical Regulators of E/I Balance for Prefrontal Cortex-Dependent Behavior and Psychiatric Disorders. Front Neural Circuits. 2018;12:37. Published 2018 May 16. doi:10.3389/fncir.2018.00037

Ghezzi F, Ngoc H, Baruchin L, Stacey J, Butt S. Sensory modality-specific GABAergic circuits reflect different timelines for emergent perception in postnatal mouse neocortex. Unpublished.

Gilissen C, Hehir-Kwa JY, Thung DT, et al. Genome sequencing identifies major causes of severe intellectual disability. Nature. 2014;511(7509):344-347. doi:10.1038/nature13394

Gómez L, Dooley J, Blumberg M. Activity in developing prefrontal cortex is shaped by sleep and sensory experience. bioRxiv 2022.07.31.502200; doi: https://doi.org/10.1101/2022.07.31.502200

Greenham LW, Greenham V. Sexing mouse pups. Lab Anim. 1977;11(3):181-184. doi:10.1258/002367777780936620

Greig LC, Woodworth MB, Galazo MJ, Padmanabhan H, Macklis JD. Molecular logic of neocortical projection neuron specification, development and diversity. Nat Rev Neurosci. 2013;14(11):755-769. doi:10.1038/nrn3586

Gruber AJ, Calhoon GG, Shusterman I, Schoenbaum G, Roesch MR, O'Donnell P. More is less: a disinhibited prefrontal cortex impairs cognitive flexibility. J Neurosci. 2010;30(50):17102-17110. doi:10.1523/JNEUROSCI.4623-10.2010

Hanganu IL, Ben-Ari Y, Khazipov R. Retinal waves trigger spindle bursts in the neonatal rat visual cortex. J Neurosci. 2006;26(25):6728-6736. doi:10.1523/JNEUROSCI.0752-06.2006

Hengen KB, Lambo ME, Van Hooser SD, Katz DB, Turrigiano GG. Firing rate homeostasis in visual cortex of freely behaving rodents. Neuron. 2013;80(2):335-342. doi:10.1016/j.neuron.2013.08.038

Hoover WB, Vertes RP. Anatomical analysis of afferent projections to the medial prefrontal cortex in the rat. Brain Struct Funct. 2007;212(2):149-179. doi:10.1007/s00429-007-0150-4

Iascone DM, Li Y, Sümbül U, et al. Whole-Neuron Synaptic Mapping Reveals Spatially Precise Excitatory/Inhibitory Balance Limiting Dendritic and Somatic Spiking. Neuron. 2020;106(4):566-578.e8. doi:10.1016/j.neuron.2020.02.015

Isaacson JS, Scanziani M. How inhibition shapes cortical activity. Neuron. 2011;72(2):231-243. doi:10.1016/j.neuron.2011.09.027

Jia X, Xing D, Kohn A. No consistent relationship between gamma power and peak frequency in macaque primary visual cortex. J Neurosci. 2013;33(1):17-25. doi:10.1523/JNEUROSCI.1687-12.2013

Khazipov R, Minlebaev M, Valeeva G. Early gamma oscillations. Neuroscience. 2013;250:240-252. doi:10.1016/j.neuroscience.2013.07.019

Kim H, Ährlund-Richter S, Wang X, Deisseroth K, Carlén M. Prefrontal Parvalbumin Neurons in Control of Attention. Cell. 2016;164(1-2):208-218. doi:10.1016/j.cell.2015.11.038

Kohn A, Zandvakili A, Smith MA. Correlations and brain states: from electrophysiology to functional imaging. Curr Opin Neurobiol. 2009;19(4):434-438. doi:10.1016/j.conb.2009.06.007

Kvitsiani D, Ranade S, Hangya B, Taniguchi H, Huang JZ, Kepecs A. Distinct behavioural and network correlates of two interneuron types in prefrontal cortex. *Nature*. 2013;498(7454):363-366. doi:10.1038/nature12176

Le Merre P, Ährlund-Richter S, Carlén M. The mouse prefrontal cortex: Unity in diversity. Neuron. 2021;109(12):1925-1944. doi:10.1016/j.neuron.2021.03.035

Lim L, Mi D, Llorca A, Marín O. Development and Functional Diversification of Cortical Interneurons. Neuron. 2018;100(2):294-313. doi:10.1016/j.neuron.2018.10.009

Martini FJ, Guillamón-Vivancos T, Moreno-Juan V, Valdeolmillos M, López-Bendito G. Spontaneous activity in developing thalamic and cortical sensory networks. Neuron. 2021;109(16):2519-2534. doi:10.1016/j.neuron.2021.06.026

Minlebaev M, Ben-Ari Y, Khazipov R. Network mechanisms of spindle-burst oscillations in the neonatal rat barrel cortex in vivo. J Neurophysiol. 2007;97(1):692-700. doi:10.1152/jn.00759.2006

Minlebaev M, Colonnese M, Tsintsadze T, Sirota A, Khazipov R. Early γ oscillations synchronize developing thalamus and cortex. Science. 2011;334(6053):226-229. doi:10.1126/science.1210574

Nahar L, Delacroix BM, Nam HW. The Role of Parvalbumin Interneurons in Neurotransmitter Balance and Neurological Disease. Front Psychiatry. 2021;12:679960. Published 2021 Jun 18. doi:10.3389/fpsyt.2021.679960

Narayanan NS, Laubach M. Delay activity in rodent frontal cortex during a simple reaction time task. J Neurophysiol. 2009;101(6):2859-2871. doi:10.1152/jn.90615.2008

Niculescu D, Lohmann C. Gap junctions in developing thalamic and neocortical neuronal networks. Cereb Cortex. 2014;24(12):3097-3106. doi:10.1093/cercor/bht175

Oren I, Mann EO, Paulsen O, Hájos N. Synaptic currents in anatomically identified CA3 neurons during hippocampal gamma oscillations in vitro. J Neurosci. 2006;26(39):9923-9934. doi:10.1523/JNEUROSCI.1580-06.2006

Pachitariu M, Steinmetz N, Kadir S, Carandini M, D. HK. Kilosort: realtime spike-sorting for extracellular electrophysiology with hundreds of channels. bioRxiv. 2016; 061481.

Parenti I, Rabaneda LG, Schoen H, Novarino G. Neurodevelopmental Disorders: From Genetics to Functional Pathways. Trends Neurosci. 2020;43(8):608-621. doi:10.1016/j.tins.2020.05.004

Pasupathy A, Miller EK. Different time courses of learning-related activity in the prefrontal cortex and striatum. Nature. 2005;433(7028):873-876. doi:10.1038/nature03287

Petersen PC, Siegle JH, Steinmetz NA, Mahallati S, Buzsáki G. CellExplorer: A framework for visualizing and characterizing single neurons. Neuron. 2021;109(22):3594-3608.e2. doi:10.1016/j.neuron.2021.09.002

Pouille F, Marin-Burgin A, Adesnik H, Atallah BV, Scanziani M. Input normalization by global feedforward inhibition expands cortical dynamic range. Nat Neurosci. 2009;12(12):1577-1585. doi:10.1038/nn.2441

Rensing N, Moy B, Friedman JL, Galindo R, Wong M. Longitudinal analysis of developmental changes in electroencephalography patterns and sleep-wake states of the neonatal mouse. *PLoS One*. 2018;13(11):e0207031. Published 2018 Nov 6. doi:10.1371/journal.pone.0207031

Riedemann T. Diversity and Function of Somatostatin-Expressing Interneurons in the Cerebral Cortex. Int J Mol Sci. 2019;20(12):2952. Published 2019 Jun 17. doi:10.3390/ijms20122952

Rossant C, Kadir SN, Goodman DFM, et al. Spike sorting for large, dense electrode arrays. Nat Neurosci. 2016;19(4):634-641. doi:10.1038/nn.4268

Rubenstein JL, Merzenich MM. Model of autism: increased ratio of excitation/inhibition in key neural systems. Genes Brain Behav. 2003;2(5):255-267. doi:10.1034/j.1601-183x.2003.00037.x

Sceniak MP, Maciver MB. Cellular actions of urethane on rat visual cortical neurons in vitro. J Neurophysiol. 2006;95(6):3865-3874. doi:10.1152/jn.01196.2005

Schindelin J, Arganda-Carreras I, Frise E, et al. Fiji: an open-source platform for biological-image analysis. Nat Methods. 2012;9(7):676-682. Published 2012 Jun 28. doi:10.1038/nmeth.2019

Schubert D, Martens GJ, Kolk SM. Molecular underpinnings of prefrontal cortex development in rodents provide insights into the etiology of neurodevelopmental disorders. Mol Psychiatry. 2015 Jul;20(7):795-809. doi: 10.1038/mp.2014.147. Epub 2014 Dec 2. PMID: 25450230; PMCID: PMC4486649.

Shen W, McKeown CR, Demas JA, Cline HT. Inhibition to excitation ratio regulates visual system responses and behavior in vivo. J Neurophysiol. 2011;106(5):2285-2302. doi:10.1152/jn.00641.2011

Shumkova, V., Sitdikova, V., Rechapov, I. *et al.* Effects of urethane and isoflurane on the sensory evoked response and local blood flow in the early postnatal rat somatosensory cortex. *Sci Rep* **11**, 9567 (2021). https://doi.org/10.1038/s41598-021-88461-8

Sohal VS. How Close Are We to Understanding What (if Anything) γ Oscillations Do in Cortical Circuits?. J Neurosci. 2016;36(41):10489-10495. doi:10.1523/JNEUROSCI.0990-16.2016

Sohal VS, Zhang F, Yizhar O, Deisseroth K. Parvalbumin neurons and gamma rhythms enhance cortical circuit performance. Nature. 2009;459(7247):698-702. doi:10.1038/nature07991

Stanley DA, Roy JE, Aoi MC, Kopell NJ, Miller EK. Low-Beta Oscillations Turn Up the Gain During Category Judgments. Cereb Cortex. 2018;28(1):116-130. doi:10.1093/cercor/bhw356

Tuncdemir SN, Wamsley B, Stam FJ, et al. Early Somatostatin Interneuron Connectivity Mediates the Maturation of Deep Layer Cortical Circuits. Neuron. 2016;89(3):521-535. doi:10.1016/j.neuron.2015.11.020

Valero M, Viney TJ, Machold R, et al. Sleep down state-active ID2/Nkx2.1 interneurons in the neocortex. *Nat Neurosci*. 2021;24(3):401-411. doi:10.1038/s41593-021-00797-6

Vanhatalo S, Kaila K. Development of neonatal EEG activity: from phenomenology to physiology. Semin Fetal Neonatal Med. 2006;11(6):471-478. doi:10.1016/j.siny.2006.07.008

Veit J, Hakim R, Jadi MP, Sejnowski TJ, Adesnik H. Cortical gamma band synchronization through somatostatin interneurons. Nat Neurosci. 2017;20(7):951-959. doi:10.1038/nn.4562

Vinck M, van Wingerden M, Womelsdorf T, Fries P, Pennartz CM. The pairwise phase consistency: a bias-free measure of rhythmic neuronal synchronization. Neuroimage. 2010;51(1):112-122. doi:10.1016/j.neuroimage.2010.01.073

Warden MR, Miller EK. Task-dependent changes in short-term memory in the prefrontal cortex. J Neurosci. 2010;30(47):15801-15810. doi:10.1523/JNEUROSCI.1569-10.2010

Wehr M, Zador AM. Balanced inhibition underlies tuning and sharpens spike timing in auditory cortex. Nature. 2003;426(6965):442-446. doi:10.1038/nature02116

Wilson CJ, Higgs MH, Simmons DV, Morales JC. Oscillations and Spike Entrainment. F1000Res. 2018;7:F1000 Faculty Rev-1960. Published 2018 Dec 20. doi:10.12688/f1000research.16451.1

Xu Q, Tam M, Anderson SA. Fate mapping Nkx2.1-lineage cells in the mouse telencephalon. J Comp Neurol. 2008;506(1):16-29. doi:10.1002/cne.21529

Yuste R. Circuit neuroscience: the road ahead. Front Neurosci. 2008;2(1):6-9. Published 2008 Aug 1. doi:10.3389/neuro.01.017.2008